Check for updates

Received: 11 September 2020 | Revised: 12 February 2021 | Accepted: 13 February 2021

DOI: 10.1111/pce.14034

ORIGINAL ARTICLE

Plant, Cell & Environment WILEY

Calm on the surface, dynamic on the inside. Molecular homeostasis of *Anabaena* sp. PCC 7120 nitrogen metabolism

Giorgio Perin[1] | Tyler Fletcher[2] | Virag Sagi-Kiss[3] | David C. A. Gaboriau[4] | Mathew R. Carey[3] | Jacob G. Bundy[3] | Patrik R. Jones[1]

[1]Department of Life Sciences, Imperial College London, London, UK

[2]Complex Carbohydrate Research Center and Department of Chemistry, University of Georgia, Athens, Georgia

[3]Department of Metabolism, Digestion and Reproduction, Imperial College London, London, UK

[4]Facility for Imaging by Light Microscopy, NHLI, Imperial College London, London, UK

Correspondence
Patrik R. Jones, Department of Life Sciences, Imperial College London, London, UK.
Email: p.jones@imperial.ac.uk

Present address
Giorgio Perin, Department of Biology, University of Padova, Padova, Italy

Funding information
BBSRC, Grant/Award Numbers: BB/N003608/1, BB/L015129/1; Wellcome Trust, Grant/Award Number: 104931/Z/14/Z

Abstract

Nitrogen sources are all converted into ammonium/ia as a first step of assimilation. It is reasonable to expect that molecular components involved in the transport of ammonium/ia across biological membranes connect with the regulation of both nitrogen and central metabolism. We applied both genetic (i.e., *Δamt* mutation) and environmental treatments to a target biological system, the cyanobacterium *Anabaena* sp PCC 7120. The aim was to both perturb nitrogen metabolism and induce multiple inner nitrogen states, respectively, followed by targeted quantification of key proteins, metabolites and enzyme activities. The absence of AMT transporters triggered a substantial whole-system response, affecting enzyme activities and quantity of proteins and metabolites, spanning nitrogen and carbon metabolisms. Moreover, the *Δamt* strain displayed a molecular fingerprint indicating nitrogen deficiency even under nitrogen replete conditions. Contrasting with such dynamic adaptations was the striking near-complete lack of an externally measurable altered phenotype. We conclude that this species evolved a highly robust and adaptable molecular network to maintain homeostasis, resulting in substantial internal but minimal external perturbations. This analysis provides evidence for a potential role of AMT transporters in the regulatory/signalling network of nitrogen metabolism and the existence of a novel fourth regulatory mechanism controlling glutamine synthetase activity.

KEYWORDS
AMT transporters, homeostasis control, nitrogen metabolism, systems biology

1 | INTRODUCTION

Cyanobacteria are a group of morphologically diverse oxygenic photosynthetic bacteria (Singh & Montgomery, 2011) almost ubiquitous to every habitat on Earth, from hot springs to Antarctic rocks (Percival & Williams, 2013). They are often found as integral members of complex ecosystems representing all three domains of life (D. G. Adams et al., 2013; D. G. Adams & Duggan, 2008), where they contribute to whole ecosystem functionality by photosynthesis-driven assimilation of nutrients. One of the key nutrients they assimilate and provide to the (local) ecosystem is nitrogen (N), an essential building block for amino and nucleic acid biosynthesis. Cyanobacteria have a variety of complementary N assimilatory pathways, including ammonium [NH_4^+ (Montesinos, Muro-Pastor, Herrero, & Flores, 1998)], nitrate [NO_3^- (Omata, Andriesse, & Hirano, 1993)] nitrite [NO_2^- (Bird & Wyman, 2003)] and urea (Valladares, Montesinos, Herrero, & Flores, 2002), and have a key role in the global nitrogen cycle (Flores & Herrero, 2005). Some genera even use amino acids [e.g., arginine and glutamine (Montesinos, Herrero, & Flores, 1997)] or directly fix atmospheric nitrogen [biological nitrogen fixation (BNF), (Herrero, Muro-Pastor, & Flores, 2001)], globally contributing 200 million

This is an open access article under the terms of the Creative Commons Attribution License, which permits use, distribution and reproduction in any medium, provided the original work is properly cited.
© 2021 The Authors. Plant, Cell & Environment published by John Wiley & Sons Ltd.

tonnes of fixed N per year (Rascio & La Rocca, 2013). Cyanobacteria are also involved in symbiotic associations, with reduced carbon delivered to cyanobacteria in order to sustain BNF (Backer et al., 2018). An example of such symbiotic associations is the aquatic fern *Azolla caroliniana*, which receives fixed N from a filamentous cyanobacterium (*Anabaena azollae*) hosted in the ovoid cavities of the plant's leaves (Lechno-Yossef & Nierzwicki-Bauer, 2005).

In their free-living form, planktonic *Anabaena* spp. make a significant contribution to the carbon and nitrogen economy of multiple ecosystems (Kellar & Goldman, 1979). *Anabaena* sp. PCC 7120 (henceforth 7120) is an isolated strain showing high genome sequence similarity with *A. azollae* and is commonly used as a model organism to investigate cyanobacterial N-fixation (Herrero, Stavans, & Flores, 2016). As nitrogenases are oxygen-sensitive, photosynthesis-driven BNF calls for spatial and/or temporal separation between the metabolic pathway fuelling energy/carbon inputs (i.e., photosynthesis) and N-fixation (Figure 1). Under diazotrophic conditions, 7120 differentiates 5–10% of its cells into specialized N-fixing heterocysts, following a highly

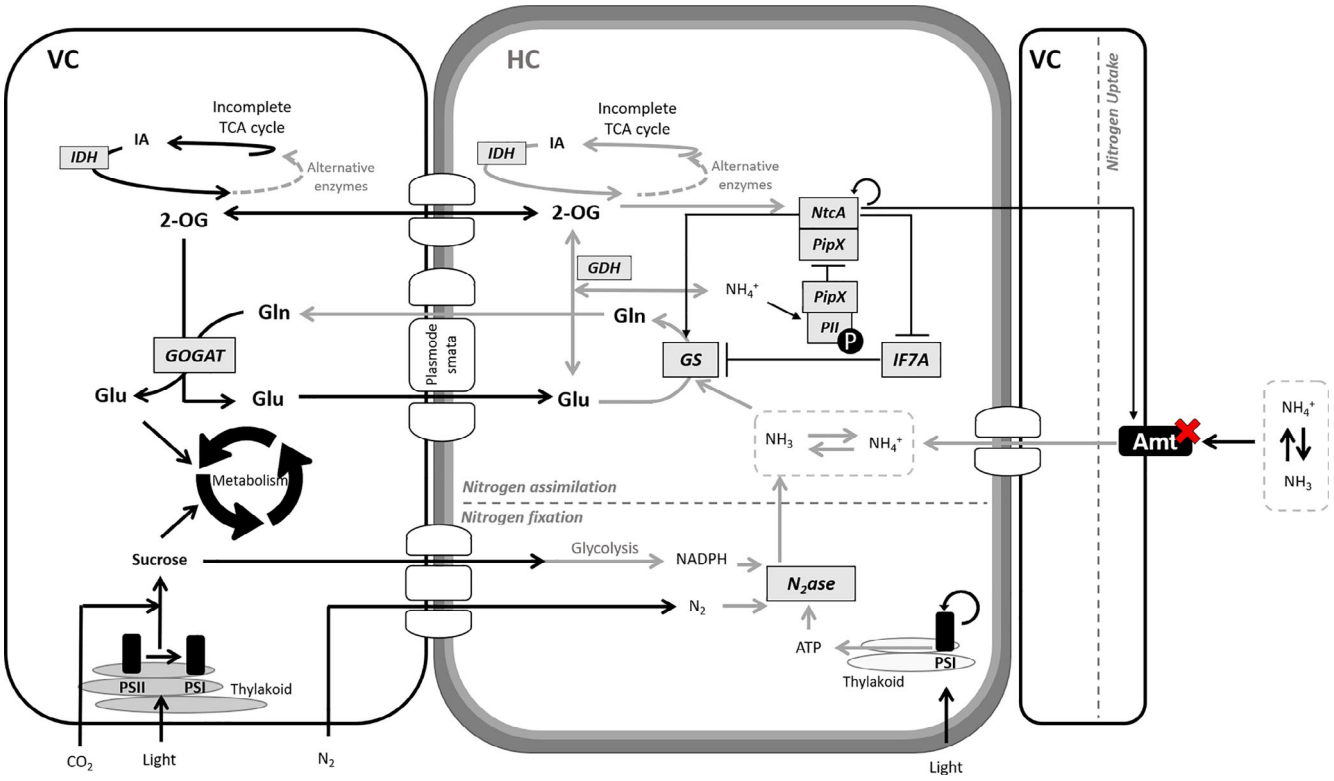

FIGURE 1 Schematic overview of major molecular players regulating N metabolism and the metabolic interaction between heterocysts (HC) and vegetative (VC) cells in *Anabaena* sp. PCC 7120, in diazotrophic conditions. Nitrogenase (N_2ase) fixes one molecule of atmospheric N_2 into two molecules of NH_3 in heterocysts (Inomura, Bragg, & Follows, 2017), using reducing power (NADPH) from the catabolism of carbon -compounds (sucrose) photosynthesized in vegetative cells (Cumino, Marcozzi, Barreiro, & Salerno, 2007; Nürnberg et al., 2015) and energy (ATP) from the residual photosynthetic activity in heterocysts [i.e., cyclic electron flow around photosystem I (PSI) (Cardona & Magnuson, 2010)]. NH_3 is then assimilated through glutamine synthetase (GS) via the amidation of glutamate (Glu) to glutamine (Gln) (Forchhammer & Selim, 2019). GS activity is controlled through posttranslational inactivation (Bolay, Muro-Pastor, Florencio, & Klähn, 2018) by IF7A (Galmozzi, Saelices, Florencio, & Muro-Pastor, 2010). Glutamate dehydrogenase (GDH) marginally contributes to the assimilation flux of fixed N, catalysing the reversible conversion of 2-oxoglutarate (2-OG) to Glu (Meeks, Wolk, & Lockau, 1978). Subsequently, in vegetative cells (Martín-Figueroa, Navarro, & Florencio, 2000), glutamine oxoglutarate aminotransferase (GOGAT) catalyses the transfer of the amine group from Gln to 2-OG, generating two molecules of Glu. As N metabolism spans different cell types, a coordinated exchange of metabolites (i.e., sucrose, Gln, Glu and 2-OG) between vegetative cells and heterocysts via septal junctions [plasmodesmata (Mullineaux et al., 2008)] is required to maintain metabolic homeostasis. 2-OG is also a metabolic intermediate of the tricarboxylic acid (TCA) cycle [synthesized from isocitric acid (IA) by isocitrate dehydrogenase (IDH)], thus connecting N and C metabolism at a central point. Cyanophycin (CPG) is a polymer playing an important role in the distribution of N among the two cell types. In this figure, CPG was omitted and we refer the reader to Figure S6 in Data S1 for a complete description of its metabolism. N metabolism homeostasis is controlled by a molecular network, including the proteins NtcA, PipX and PII. When external N is available, PII is not phosphorylated and it sequesters PipX, preventing its biding to NtcA and consequently its activation. When N is limiting, PII is phosphorylated, freeing PipX, which ultimately binds and activates NtcA (Valladares et al., 2011). The red cross indicates the knock-out (KO) mutant Δamt used in this work (Paz-Yepes, Merino-Puerto, Herrero, & Flores, 2008). In this simplified scheme, we localized AMT transporters in the membrane of vegetative cells, according to Merino-Puerto, Mariscal, Mullineaux, Herrero, and Flores (2010)). Major molecular players targeted in this work are highlighted by a grey square or in bold, respectively for proteins and metabolites [Colour figure can be viewed at wileyonlinelibrary.com]

regulated developmental pattern [i.e., a single heterocyst every 10–20 cells (Kumar, Mella-Herrera, & Golden, 2010)]. Heterocysts undergo a deep metabolic and structural remodelling to enable efficient N-fixation (Golden & Yoon, 1998). The oxygen-evolving photosystem II (PSII) is dismantled, carbon fixation is avoided, photorespiratory activity is increased during differentiation (Valladares, Maldener, Muro-Pastor, Flores, & Herrero, 2007), flavodiiron proteins catalyse the reduction of molecular oxygen to water (Ermakova et al., 2014) and cells are surrounded by a thicker cell envelope [through the deposition of two additional envelope layers, that is, an inner glycolipids and an outer polysaccharides layer (Nicolaisen, Hahn, & Schleiff, 2009)] than the vegetative cells, all contributing to the required microoxic environment for N-fixation activity (Kumar et al., 2010) (Figure 1).

Heterocysts and vegetative cells have complementary metabolism, with the former providing fixed nitrogen and the latter returning reduced carbon needed to sustain BNF (Malatinszky, Steuer, & Jones, 2017). This metabolic exchange and associated networks (summarized in Figure 1) are most likely carefully coordinated in order to ensure organism-level homeostasis (Mullineaux et al., 2008). The question is, how does this molecular coordination take place?

In many organisms, including 7120, N metabolism is orchestrated by a complex signalling network with the likely aim to balance the cellular C/N ratio (Forchhammer & Selim, 2019). N and C metabolisms are in fact tightly coupled as (a) the two elements are among the four most abundant in living organisms (i.e., oxygen, carbon, hydrogen and nitrogen, respectively), calling for coordination to avoid metabolic inefficiencies, and (b) N assimilation depends on the availability of C skeleton, with shortage or oversupply strongly affecting the metabolism of N (Zhang, Zhou, Burnap, & Peng, 2018). Therefore, a properly balanced N and C metabolism is necessary for optimal growth and different levels of regulation exist to control uptake and assimilation efficiencies of both chemical species. When the C source (i.e., CO_2 in case of phototrophic metabolism) is not limiting, the regulatory mechanisms controlling C/N balance depend on both the abundance and the nature of the N sources available to the cell. Although cyanobacteria can use multiple N sources, including NH_4^+, intracellularly they are all converted to NH_4^+, the most reduced and energetically favourable N source (Robinson, 2017). Ammonia translocation across biological membranes is actively driven by AMT transporters that belong to a family of permeases widely distributed in living organisms (Javelle et al., 2007), or through passive diffusion if the external pH pushes the equilibrium towards the uncharged form (NH_3, ammonia). In addition, AMT proteins are also known to be involved in the regulation of N metabolism, at least in some bacteria species (Arcondeguy, Jack, & Merrick, 2001). As an example, in the purple bacterium *Rhodobacter capsulatus*, AMT proteins are implicated in (a) the post-translational regulation of nitrogenase, driven by a direct interaction between AmtB and GlnK (a homolog of PII) (Tremblay & Hallenbeck, 2008), and (b) the regulation of GS activity during the switch towards diazotrophic conditions (Yakunin & Hallenbeck, 2002). Also in cyanobacteria [e.g., *Synechocystis* sp. PCC 6803 (Watzer et al., 2019)] AMT proteins were found to directly interact with the PII protein to prevent intracellular accumulation of ammonium/ia. 7120 bears a gene cluster including three *amt* genes, namely *amt4*, *amt1* and *amtB* (Paz-Yepes et al., 2008). In this work, we used a knock-out (KO) mutant of the whole gene cluster in 7120 [henceforth Δamt (Paz-Yepes et al., 2008)] with the aim to investigate how a N_2-fixing cyanobacterium responds to perturbation of N-metabolism at a whole-system level. Although several genes and proteins in 7120 have been individually studied previously (Flores & Herrero, 2005; Forchhammer & Selim, 2019), it is difficult to make over-arching conclusions on the regulatory system, also as cyanobacteria differ substantially relative to heterotrophic bacteria (Bolay et al., 2018; Reitzer, 2003). The aim of this work is also to enhance our understanding that contributes towards the practical goal of eventually rerouting N metabolism for biotechnological purposes (Perin, Yunus, Valton, Alobwede, & Jones, 2019).

2 | RESULTS

2.1 | AMT transporters are not required to support growth of 7120 under constant laboratory conditions but still play a role in N metabolism

Phototrophic growth of 7120 WT and Δ*amt* strains was carried out in media with different N sources (NO_3^-, N_2 and NH_4^+) at saturating CO_2 (i.e., 1%), in order to avoid C limitation. Such conditions are expected to vary the internal C/N balance by modifying the abundance and nature of the N source. The Δ*amt* mutant did not display an altered growth phenotype with respect to the parental strain, regardless of the N source (Figure 2A), confirming that the whole *amt* cluster is not necessary to support growth of 7120 under the tested laboratory conditions (Paz-Yepes et al., 2008).

Growth in atmospheric N_2 lags behind both NO_3^- and NH_4^+, with cells taking ~48 hr to fully switch to atmospheric N_2 fixation. Growth in NH_4^+ shows two distinct modes, as indicated by the specific growth rate (Figure S2 in Data S1), suggesting that 5 mM NH_4^+ is not enough to support maximal growth (i.e., growth in NO_3^- in this experiment) over the whole experimental time frame, and that it likely runs out after ~48 hr (Figure 2A). The nitrogenase activity, measured after 96 hr, confirms that 5 mM NH_4^+ runs out over the course of the experiment, triggering diazotrophic growth (Figure 2B). Moreover, the lower nitrogenase activity with respect to N_2 conditions highlights that cells in $NH4^+$ media, at the time of sampling, are in a transitory phase before reaching the maximal N fixation potential. Interestingly, in $NH4^+$ media, the Δ*amt* strain shows a higher nitrogenase activity per unit of chlorophyll (Chl) than the parental strain, although that does not result in an improvement in growth, suggesting possible compensatory modifications in the following metabolic steps (e.g., N assimilation). After 96 hr, GS activity, a (supposed) central player in N metabolism in this organism (Bolay et al., 2018), is also affected by the mutation (as in the case of fully diazotrophic conditions [N_2] in which Δamt strain shows a greater N assimilation activity than the WT, see Figure 2C). Moreover, when both strains are grown in N_2, GS activity

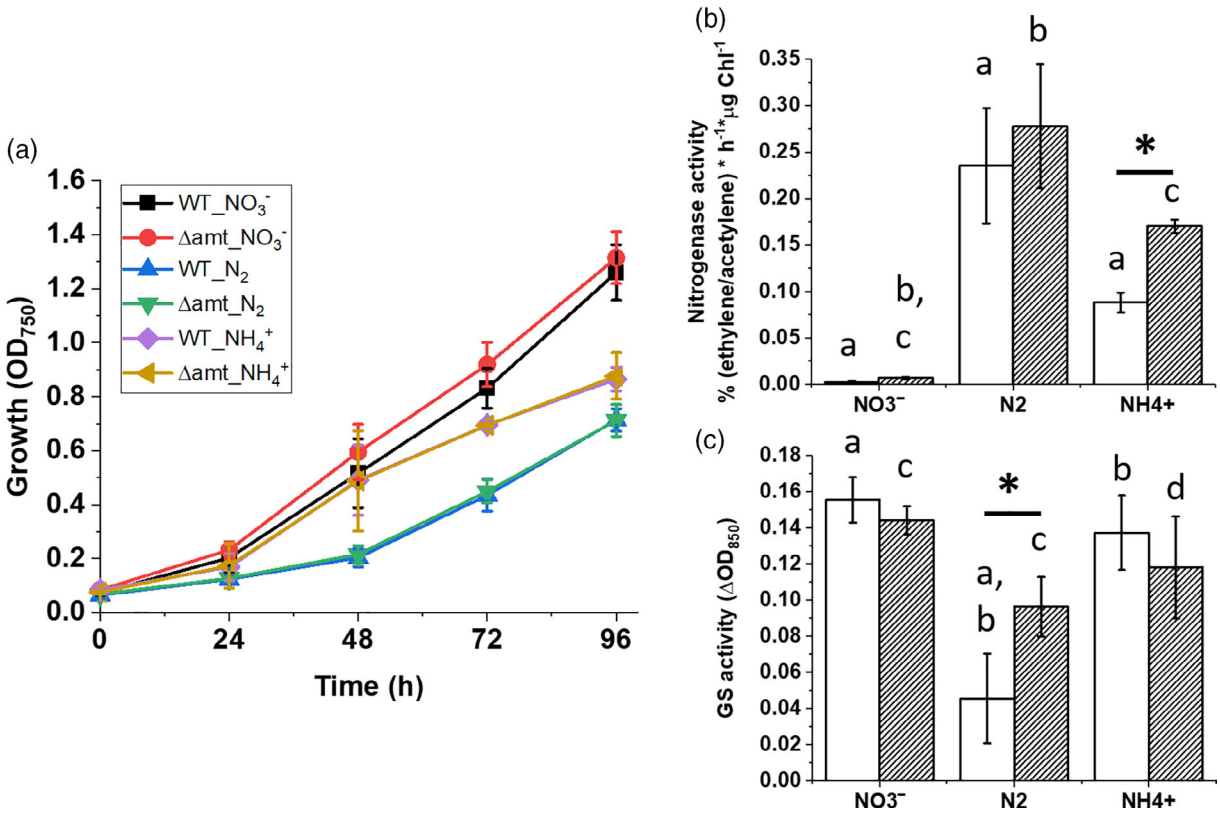

FIGURE 2 Growth of 7120 WT and Δamt strains with different N sources. The two strains were cultivated in different N sources for 96 hr. Growth (A) was monitored over the course of the whole experiment, while nitrogenase activity (B) and GS activity (C) were measured after 96 hr in such cultivation conditions. Data are indicated as average ± *SD* of six biological replicates. Statistically significant differences between WT (white bars) and Δamt (striped bars) are indicated with an asterisk, while the same alphabet letter indicates statistically significant differences for the same strain in different growth conditions (one-way ANOVA, *p*-value <.05) [Colour figure can be viewed at wileyonlinelibrary.com]

is overall lower than in the other two growth conditions. The collective data indicated that the loss of AMT resulted in no phenotypic change, but that N-metabolism had adjusted, presumably to maintain homeostasis, raising the following question: how extensive was this adaption and what molecular players were involved?

In 7120, GS is regulated both transcriptionally and post-translationally, according to the C/N status of the cell (Bolay et al., 2018). The abundance of the protein is transcriptionally controlled and changes according to the N source(s) as observed in the WT strain, but not in Δ*amt* (Figure 3A).

The abundance of GS (Figure 3A) does not reflect its measured activity (Figure 2C). GS activity is known to be controlled by covalent binding of the inactivation factor IF7A, in response to the C/N balance of the cell (Galmozzi et al., 2010). As shown in Figure 3B, there is a statistically significant negative correlation between GS activity and the amount of its inactivation factor IF7A for both strains across different N sources. However, the *Δamt* mutant shows a weaker correlation between GS activity and IF7A abundance than the parental strain (WT, Pearson correlation −.72, *p*-value .02, Student's *t* test; Δ*amt*, Pearson correlation −.55, *p*-value .001, Student's *t* test; Table S1 in Data S1), suggesting other molecular players also contribute to the regulation of GS activity in this organism. The absence of AMT transporters has an effect on the IF7A/GS activity relationship (Figure 3B). In N replete conditions (NO_3^-), there is no difference between the two strains, whilst under the two other N deplete conditions, the deletion of *amt* results in a divergence between the two strains (Figure 3B). The genetic and environmental treatments affect GS activity through a combined variation in both GS and IF7A abundance (Figure 3A and Figure S3 in Data S1). In particular, it is worth noting that Δ*amt* retains GS activity even if the amount of IF7A changes, supporting the idea that other regulatory players also may be involved. Based on the available data, we hypothesised that AMT transporters are directly or indirectly involved in the regulation of GS activity during the switch towards diazotrophic conditions in 7120, as already observed in the purple bacterium *R. capsulatus* (Yakunin & Hallenbeck, 2002).

2.2 | AMT transporters may be involved in the signalling and/or regulation of N metabolism in 7120

In order to test this hypothesis, the internal metabolic changes taking place in 7120 WT and Δ*amt* during the transition from N replete to deplete conditions were followed by combining physiological data with targeted proteomic and metabolomic quantification of molecular players known to be involved in the regulation of N metabolism in

7120 (Figure 1). Both WT and Δ*amt* strains were cultivated in $BG11_0$ supplemented with 5 mM NH_4^+. The concentration of ammonium/ia in the media and cell growth was monitored over time (Figure 4A). Four different time points were chosen to investigate the physiological and metabolic status of the cells [i.e., NR (N replete conditions), ND1, ND2 and ND4 (1, 2 and 4 days, respectively, after N depletion),

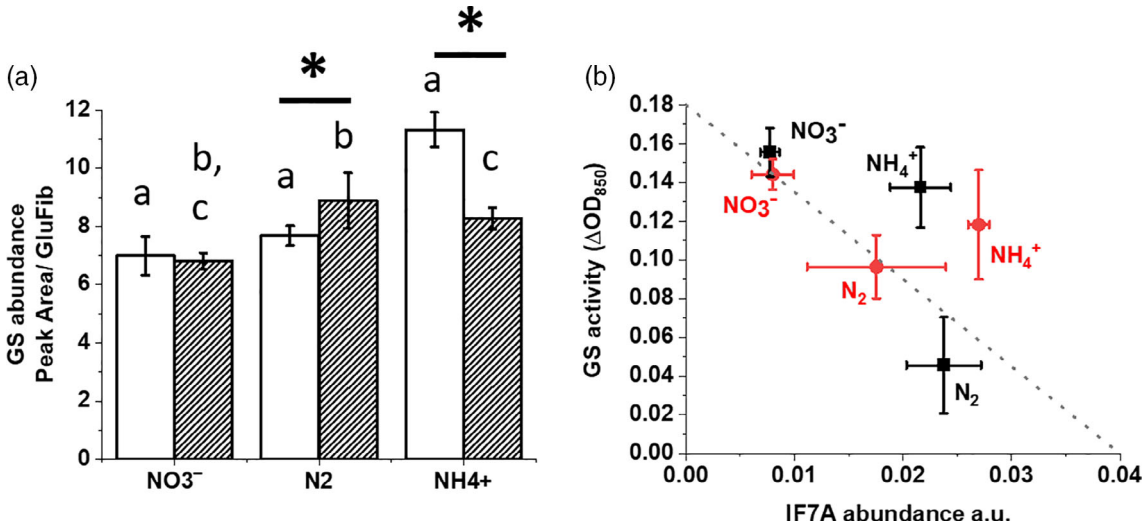

FIGURE 3 GS abundance and correlation between GS activity and IF7A amount for 7120 WT and Δamt strains, after 96 hr in the growth conditions of Figure 2a. In (A), GS abundance in the two strains is indicated after cultivation for 96 hr in the three different nitrogen sources tested in this work. In (B), the correlation between GS activity (i.e., *y*-axis, as indicated in Figure 2C) and IF7A abundance (i.e., *x*-axis) is indicated, for the same time point and different nitrogen sources tested in this work. IF7A quantification data are reported in Figure S3 in Data S1. Data are indicated as average ± *SD* of six biological replicates. Statistically significant differences between WT (white bars and black squares) and Δamt (striped bars and red circles) are indicated with an asterisk, while the same alphabet letter indicates statistically significant differences for the same strain in different growth conditions (one-way ANOVA, *p*-value <.05). In panel (B), the Pearson coefficient was calculated to assess the correlation between GS activity and IF7A abundance in both strains and the Student's *t* test was employed to assess the significance of the correlation, with the following results: WT, Pearson correlation −.72, *p*-value .02, Student's *t* test; Δamt, Pearson correlation −.55, *p*-value .001, Student's *t* test. The correlation analysis is detailed in Table S1 in Data S1 [Colour figure can be viewed at wileyonlinelibrary.com]

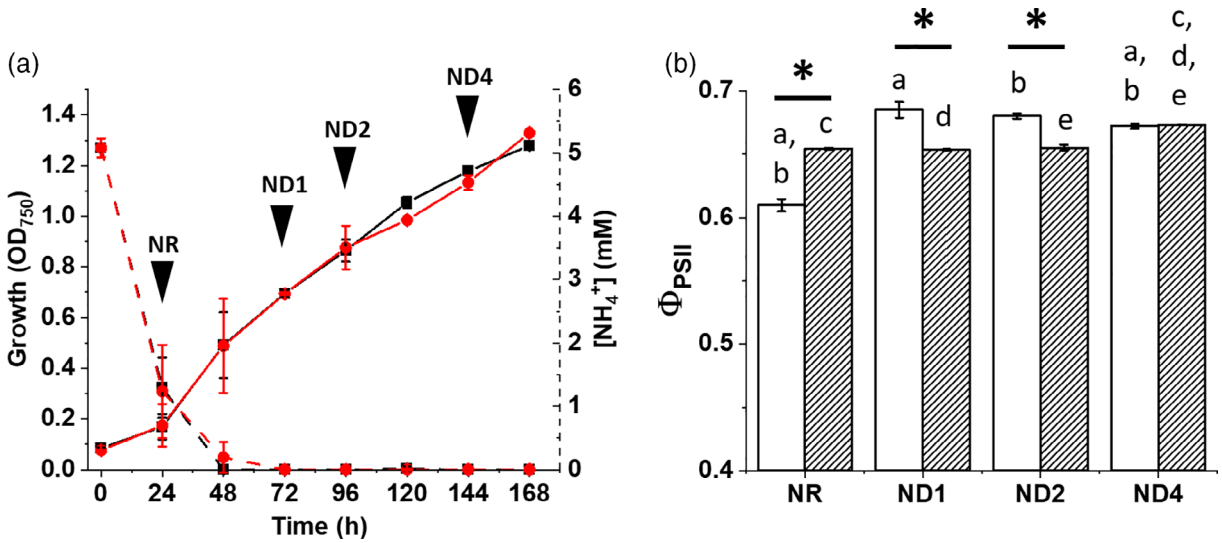

FIGURE 4 Growth, ammonium/ia consumption (A) and maximal photosynthetic efficiency [(Φ_{PSII}), (B)] monitoring for 7120 WT and Δamt strains in $BG11_0$ + 5 mM NH_4^+. In (a), black and red solid and dashed lines indicate growth and ammonium/ia concentration over time for 7120 WT and Δamt strains, respectively. Cultures were sampled at four time points over the course of the experiment [NR (Nitrogen Replete), ND1, ND2 and ND4, respectively 1, 2 and 4 days after Nitrogen Deprivation]. Data are indicated as average ± *SD* of six biological replicates. Statistically significant differences between WT (black squares and white bars) and Δamt (red circles and striped bars) are indicated with an asterisk, while the same alphabet letter indicates statistically significant differences for the same strain in different growth conditions (one-way ANOVA, *p*-value <.05) [Colour figure can be viewed at wileyonlinelibrary.com]

corresponding to 24, 72, 96 and 144 hr from the start of the experiment]. Former studies in 7120 mainly focused on the first 24 hr after N deprivation (Galmozzi et al., 2010; Valladares et al., 2011), as heterocyst differentiation is expected to occur within such time frame (Valladares et al., 2011). Here, instead, we opted for an extended sampling protocol in order to complement the information already available in literature with the knowledge of the metabolic/proteomic adjustments happening over a longer time-scale.

The absence of the whole *amt* cluster does not affect the ammonium/ia consumption rate, indicating other uptake systems or the diffusion of ammonia are enough to sustain growth in 7120, both in the first 48 hr when ammonium is present in sufficient amount (i.e., mM concentration) and after 48 hr when the culture is depleted of measurable ammonium (Figure 4A). This is in line with earlier studies indicating that AMT transporters are only expected to be involved in ammonium uptake at low pH (<7) and in limiting concentrations [i.e., μM, (Boussiba & Gibson, 1991; Paz-Yepes, Herrero, & Flores, 2007)]. It is in fact worth noting that we started the experiment providing a sufficient amount of ammonium/ia (i.e., mM concentration) to the cultures and for the first 48 hr we are thus not in condition to maximize the uptake activity of AMT transporters. The data also confirms that 5 mM NH_4^+ is not enough to support maximal growth in 7120 over a longer 96 hr culture (Figure 2A). Over the course of the experiment, both strains mostly showed a stable pigment content, suggesting the switch towards diazotrophic conditions does not unbalance the overall N status of the cell (Murton et al., 2017) (Table 1).

However, the Δ*amt* strain shows a greater Chl/Car ratio, mainly achieved through the accumulation of a higher Chl content than the parental strain (Table 1). This effect on the pigment composition has also a consequence on the photosynthetic performances. The photosynthetic activity in the parental strain changes over the course of the experiment, whilst in Δ*amt* it is more stable (Figure 4A). Moreover, the mutant shows a higher photosynthetic efficiency than WT in N replete conditions, while the difference reverses both after 24 and 48 hr under N deprivation conditions and ultimately disappears after 96 hr (Figure 4B). Given that the Δ*amt* mutation does not trigger an altered growth phenotype, whilst there are substantial changes to both photosynthesis and N metabolism, we hypothesised that the deletion of the whole *amt* cluster is in fact triggering a whole cell metabolic response in order to maintain homeostasis.

In order to validate this unanswered hypothesis, we investigated the N metabolism of 7120 more closely, targeting the same proteins and enzymatic reactions as above, but this time measured in the same time intervals as indicated in Figure 4A. Both WT and Δ*amt* strains activate N fixation (Figure 5A) as a consequence of ammonium/ia deprivation (Figure 4A). The Δ*amt* strain shows a higher nitrogenase activity than the parental strain in both ND1 and ND2, indicating a faster response to N deprivation (Figure 5A). Abundance of NifK and NifD, encoding for α and β subunits of nitrogenase, is higher in the mutant strain (Figure 5b,C, respectively), suggesting increased N fixation activity depends at least in part on a greater accumulation of the protein complex, given also the number of heterocysts over the course of the experiment is not affected by the mutation (Figure S4 in Data S1). The increased N-fixation activity does not translate to a greater growth rate in the mutant, however, suggesting possible compensatory modifications in downstream steps of N metabolism.

TABLE 1 Pigment content of WT and Δamt strains during the switch from N replete to deplete conditions

	WT	Δamt
Chl content (μg/OD_{750})		
NR	13.36 ± 0.49^{a}	14.14 ± 0.55^{d}
ND1	13.41 ± 0.18^{b}	13.38 ± 0.41^{e}
ND2	12.37 ± 0.37^{*,a,b,c}	14.26 ± 0.27^{*,e}
ND4	14.49 ± 0.72^{*,c}	16.13 ± 0.41^{*,d,e}
Car content (μg/OD_{750})		
NR	5.78 ± 0.2^{*,a}	4.73 ± 0.22^{*,c}
ND1	4.84 ± 0.05^{a,b}	4.7 ± 0.13^{d}
ND2	4.49 ± 0.12^{a,b}	4.76 ± 0.11^{e}
ND4	5.54 ± 0.29^{b}	5.86 ± 0.18^{c,d,e}
Chl/Car		
NR	2.31 ± 0.005^{*,a}	2.99 ± 0.02^{*,c}
ND1	2.77 ± 0.01^{*,a}	2.85 ± 0.01^{*,c,d}
ND2	2.75 ± 0.01^{*,b}	2.99 ± 0.01^{*,d}
ND4	2.61 ± 0.009^{*,a,b}	2.75 ± 0.01^{*,c,d}

Note: Cultures were sampled at four time points over the course of the experiment [NR (Nitrogen Replete), ND1, ND2 and ND4, respectively 1, 2 and 4 days after Nitrogen Deprivation], according to Figure 4A. Data are indicated as average ± *SD* of six biological replicates. Statistically significant differences between WT and Δamt are indicated with an asterisk, whilst the same alphabet letter indicates statistically significant differences for the same strain in different growth conditions (one-way ANOVA, *p*-value <.05).

Once atmospheric N is fixed into ammonium/ia, the latter is incorporated into amino acid metabolism. GS activity was strongly regulated in both strains also in this experiment, as observed before (Figure 2B). In N replete conditions, Δ*amt* showed greater N assimilation activity than the parental strain (i.e., NR in Figure 6A), likely to be the cause of the increased influx of N in the central metabolism, as indicated by the increased pigment content and photosynthetic activity observed in NR conditions (Table 1 and Figure 4B). Consequently, GS activity was influenced by the change in N metabolism, especially in the earlier samples. GS activity was at first reduced and then strongly increased (i.e., ND1 and ND2 in Figure 6A), before stabilising again to the same rate observed under N replete conditions (i.e., ND4 in Figure 6A). The trend in GS activity appeared to depend on the abundance of both GS and IF7A (Figure 6B,C, respectively), which accumulate differentially in the two strains. It is worth noting that in this experiment, the negative correlation between GS activity and IF7A abundance is not significant in the parental strain, whilst there is a significant correlation in the mutant genetic background (Figure 6D; WT, Pearson correlation −.77, *p*-value .13, Student's *t* test; Δ*amt*, Pearson correlation −.63, *p*-value .03, Student's *t* test; Table S1 in Data S1). This analysis confirms the hypothesis that other

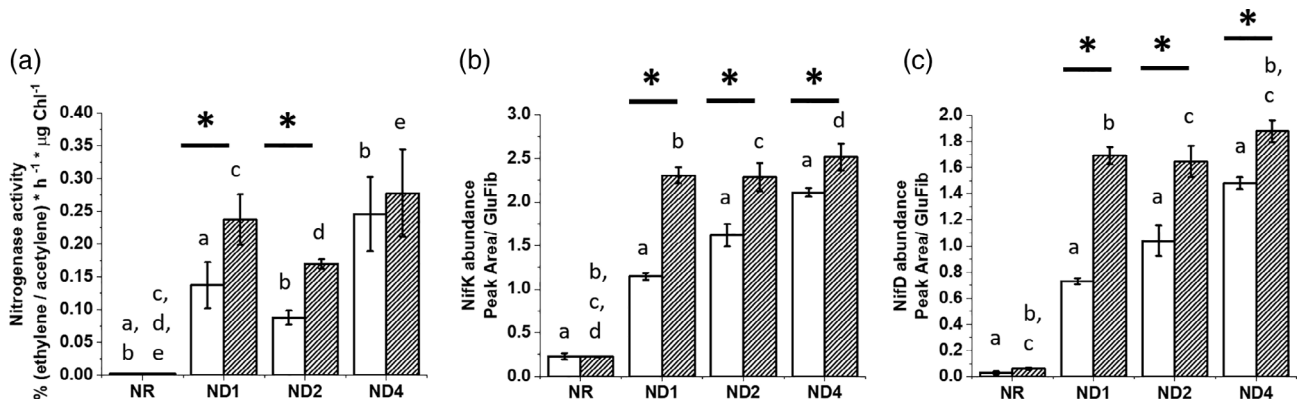

FIGURE 5 Nitrogenase activity (A), NifK (B) and NifD (C) abundance in both WT and Δamt strains, following N deprivation. Time points are those indicated in Figure 4A and correspond to NR (Nitrogen Replete), ND1, ND2 and ND4, respectively 1, 2 and 4 days after Nitrogen Deprivation. Data are indicated as average ± *SD* of six biological replicates. Statistically significant differences between WT (white bars) and Δamt (striped bars) are indicated with an asterisk, while the same alphabet letter indicates statistically significant differences for the same strain in different growth conditions (one-way ANOVA, *p*-value <.05)

compensatory molecular mechanisms controlling GS activity might exist in this species and that the latter might come into play, as a consequence of the N status of the cell. Moreover, the deletion of the whole *amt* cluster strongly affects the abundance of both GS and IF7A, which impact the overall regulation of GS activity, as the GS activity is similar across several different treatments even though the amount of IF7A varies (Figure 6D). These results strengthen the hypothesis that AMT transporters might play a direct or indirect IF7A-independent role on the GS activity in 7120.

GS is the major entry point of fixed N in the central metabolism of 7120 (Bolay et al., 2018). Nevertheless, other enzymes control the availability of GS substrates, thus indirectly contributing to the regulation of N assimilation. These include GOGAT (responsible for the regeneration of Glu in the GS-GOGAT cycle), IDH (responsible for the synthesis of 2-OG, a substrate of GOGAT) and GDH (involved in the reversible conversion between Glu and 2-OG) (Bolay et al., 2018; Forchhammer & Selim, 2019; Martín-Figueroa et al., 2000). Under the tested experimental conditions, the deletion of the whole *amt* cluster had major consequences also on the abundance of such enzymes (Figure S5 in Data S1). GOGAT accumulation followed the same trend in both strains over the course of the experiment (i.e., strong down-regulation, as a consequence of N deprivation, Figure S5A in Data S1), while IDH and GDH displayed different trends in the two genetic backgrounds (Figure S5B,C in Data S1, respectively). These observations support the notion that the absence of AMT transporters triggers both direct and indirect effects on N metabolism in 7120.

2.3 | The absence of AMT transporters affects the master regulatory network of N metabolism

Given the impact of Δ*amt* on both GS and nitrogenase, the question is how widespread the adjustments had rippled further into the cellular system? In order to address this question, we investigated the N metabolism more deeply, with an expanded number of protein quantification targets. The C/N balance of the cell is in fact also known to regulate the interaction between NctA, PipX and PII in 7120 (Forchhammer & Selim, 2019), which are expected to be the major molecular players controlling the metabolic remodelling in response to both the nature and availability of N source in the external environment, in 7120 (Figure 1). The transcription factor NtcA, active mostly once bound to PipX, regulates the abundance of nitrogenase, GS and IF7A (Picossi, Flores, & Herrero, 2014). As Δ*amt* both responds to N deprivation more quickly than the parental strain, by activating faster N-fixation (Figure 5), and also shows major alterations in the regulation of N assimilation (greater GS activity), we wondered whether the mutation might have an effect on such master molecular regulators, which control both enzymatic steps in this species (i.e., NtcA, PII and PipX, Figure 1) and we thus quantified their abundance (Figure 7).

Overall, Δ*amt* accumulated more of the three proteins over the course of the experiment relative to the parental strain, suggesting the absence of AMT transporters has an extensive impact on the cellular system, involving the master regulatory network of N metabolism. This might explain the more rapid activation of N-fixation in response to N deprivation and also the effect on N assimilation, discussed above (Figures 5 and 6). Moreover, while the abundance of the three proteins does not vary much over the course of the experiment in WT, PII does respond to N deprivation and is more abundant under NR conditions in Δ*amt* (Figure 7B). This suggests PII might be degraded after induction of N deprivation, possibly as a consequence of a greater phosphorylation rate (see Figure 1 for the molecular mechanisms controlling PII/PipX interaction). These results strengthen the notion that AMT transporters might play a central role in the signalling/regulation of N metabolism in 7120.

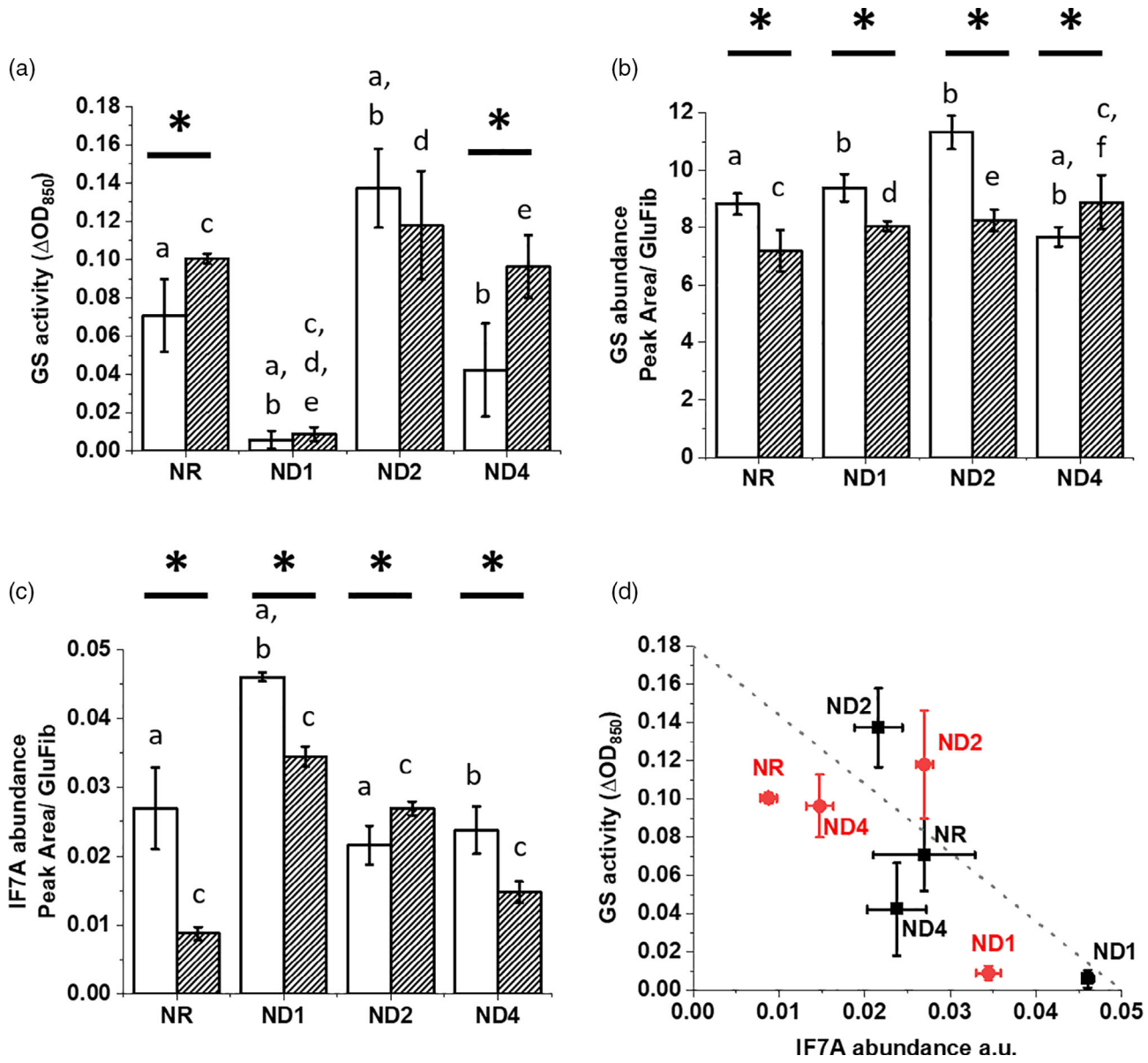

FIGURE 6 Regulation of N assimilation during the switch towards N deprivation in both 7120 WT and Δamt strains. (A) GS activity; (B) GS abundance; (C) IF7A abundance; (D) correlation between GS activity and IF7A abundance. Time points are those indicated in Figure 4A and correspond to NR (Nitrogen Replete), ND1, ND2 and ND4, respectively 1, 2 and 4 days after Nitrogen Deprivation. Data are indicated as average ± *SD* of six biological replicates. Statistically significant differences between WT (white bars and black squares) and Δamt (striped bars and red circles) are indicated with an asterisk, while the same alphabet letter indicates statistically significant differences for the same strain in different growth conditions (one-way ANOVA, *p*-value <.05). In panel (D), the Pearson coefficient was calculated to assess the correlation between GS activity and IF7A abundance in both strains and the Student's *t* test was employed to assess the significance of the correlation, with the following results: WT, Pearson correlation −.77, *p*-value .13, Student's *t* test; Δamt, Pearson correlation −.63, *p*-value .03, Student's *t* test. The correlation analysis is detailed in Table S1 in Data S1 [Colour figure can be viewed at wileyonlinelibrary.com]

2.4 | Metabolic remodelling as a consequence of *amt* deletion

Under diazotrophic conditions, coordinated metabolic interaction between vegetative cells and heterocysts is seminal for optimal growth. The absence of AMT transporters triggered an extensive remodelling at the protein level in 7120, spanning both cell types, given some of the proteins investigated in this work are known to be exclusively expressed in one of the two cell types [e.g., GOGAT in vegetative cells (Martín-Figueroa et al., 2000)]. We therefore wondered whether the same also happens at the metabolite pool level. Cyanobacteria evolved the ability to store assimilated N in the form of cyanophycin granule polypeptide (CPG), possibly acting as a buffer to naturally varying N-fixation due to fluctuations in N supply and day/night cycles (Watzer & Forchhammer, 2018). It is however worth noting that the amount of CPG in *Anabaena* is expected to reach at

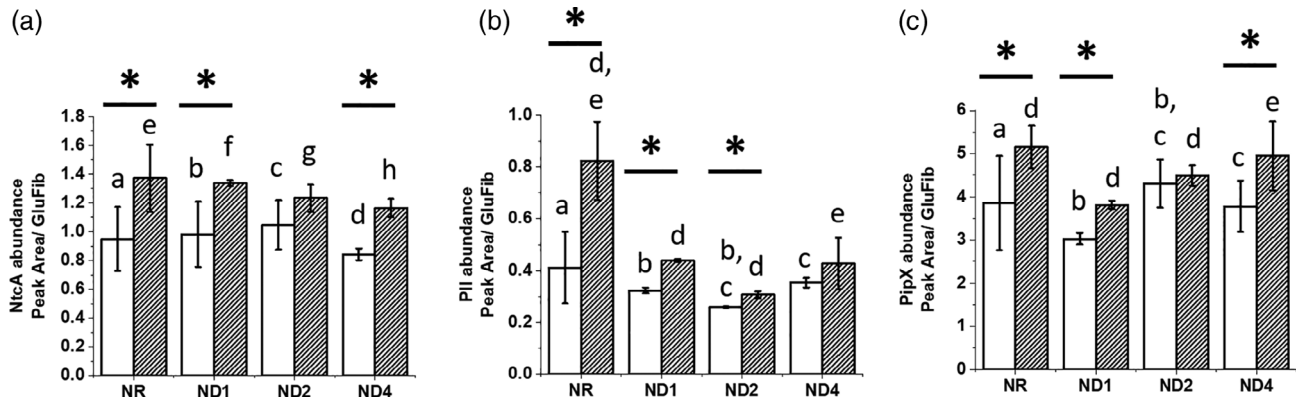

FIGURE 7 Abundance of the three major molecular players regulating N metabolism in 7120. (A). NtcA; (B). PII; (C). PipX. Time points are those indicated in Figure 4A and correspond to NR (Nitrogen Replete), ND1, ND2 and ND4, respectively 1, 2 and 4 days after Nitrogen Deprivation. Data are indicated as average ± *SD* of six biological replicates. Statistically significant differences between WT (white bars) and Δamt (striped bars) are indicated with an asterisk, while the same alphabet letter indicates statistically significant differences for the same strain in different growth conditions (one-way ANOVA, *p*-value <.05)

best 10% of the dry weight of the cell, whilst proteins accumulate up to 60% of the cell dry weight (Simon, 1973). Therefore, the major sink of nitrogen in *Anabaena* is proteins, rather than CPG. Nevertheless, in heterocystous filamentous cyanobacteria, CPG accumulates at the contact sites between heterocysts and adjacent vegetative cells and is expected to regulate the transfer of fixed N from the former to the latter (Burnat, Herrero, & Flores, 2014), thus influencing metabolite exchange between the two cell types (see Figure S6 in Data S1 for a schematic overview of CPG metabolism in 7120). In order to investigate whether the metabolites exchange between the two cell types was also affected by the mutation, we studied potential alterations in the CPG metabolism (Figure 8).

Under the tested experimental conditions, both strains accumulated CPG in NR conditions as expected (Forchhammer & Watzer, 2016) and they showed the same CPG content (Figure 8A), suggesting the deletion of AMT transporters did not perturb N storage to the point of affecting CPG accumulation. Nevertheless, the abundance of three out of four major enzymes controlling CPG metabolism (Figure S6 in Data S1) is significantly different between the two strains, with cyanophycin synthetase (CphA1), cyanophycin synthetase 2 (CphA2) and isoaspartyl dipeptidase (ISO) showing increased accumulation in the mutant with respect to the parental strain in NR (Figure 8B,D,E). We therefore hypothesized that the overall CGP metabolic flux is accelerated in the mutant under NR conditions, possibly enabling a faster response to environmental changes. When cells experience N deprivation, the cyanophycin content decreases, presumably as it is rapidly used as N source (Forchhammer & Watzer, 2016) (i.e., after 1 day of N deprivation CPG is fully consumed, Figure 8A). Nevertheless, while CPG starts building up again in the parental strain after 2 days of N deprivation, a constant consumption trend is observed over the course of the experiment in the mutant (Figure 8A). This suggests that N fixation in the WT exceeds metabolic needs and a fraction of the assimilated N is thus stored as CPG, while in the mutant this trend is disrupted. Out of the four major enzymatic steps controlling CPG metabolism in 7120, CphA1, the major enzyme controlling CPG biosynthesis (Forchhammer & Watzer, 2016), is most affected by N deprivation (Figure 8B–E), with the mutant showing a faster reduction in its abundance than the parental strain (Figure 8B). It is also worth noting that CphA2, a truncated version of CphA1 catalysing the direct recycling of the β-aspartyl-arginine dipeptide into CPG [Figure S6 in Data S1 (Forchhammer & Watzer, 2016)], is more abundant in the mutant strain in all time points (Figure 8D), strengthening the notion that CPG metabolism is accelerated in Δ*amt*.

The regulation of CPG accumulation in N fixing cyanobacteria is mediated by PII which in turn regulates N-acetyl-N-glutamate kinase (NAGK) activity (Forchhammer & Selim, 2019). NAGK catalyses the conversion of N-acetyl-L-glutamate to N-acetyl-L-glutamyl-phosphate, which is further converted to ornithine, from where Arg, the end-product of the pathway, is derived. Therefore, CPG biosynthesis directly follows the concentration of free Arg in the cell, as a consequence of feedback inhibition of NAGK (Watzer et al., 2015). In our experimental conditions, the free Arg concentration indeed strongly decreased upon N deprivation in both strains (Figure 9A,B), confirming the strong reduction in CPG content upon N deprivation, observed before (Figure 8A).

Overall, both strains display a reduction in the whole pool of free amino acids as a consequence of N deprivation (Figure 9A,B), likely suggesting a faster turnover upon N-fixing conditions. Nevertheless, upon N deprivation, the Δ*amt* strain also shows substantial remodelling of the free amino acid pools (Figure 9B), relative to the parental strain (Figure 9A). Major amino acids affected by the mutation are Lys and Asn, which display a stronger reduction in the mutant upon N deprivation, followed by Thr, Trp, Arg, Gly, Ala and Asp (Figure 9B), which instead show minor but still relevant alterations. These results indicate a comprehensive impact on the amino acid metabolism in 7120, as a consequence of the mutation. It is also worth noting the pool of acetyl-lysine is differentially regulated in the

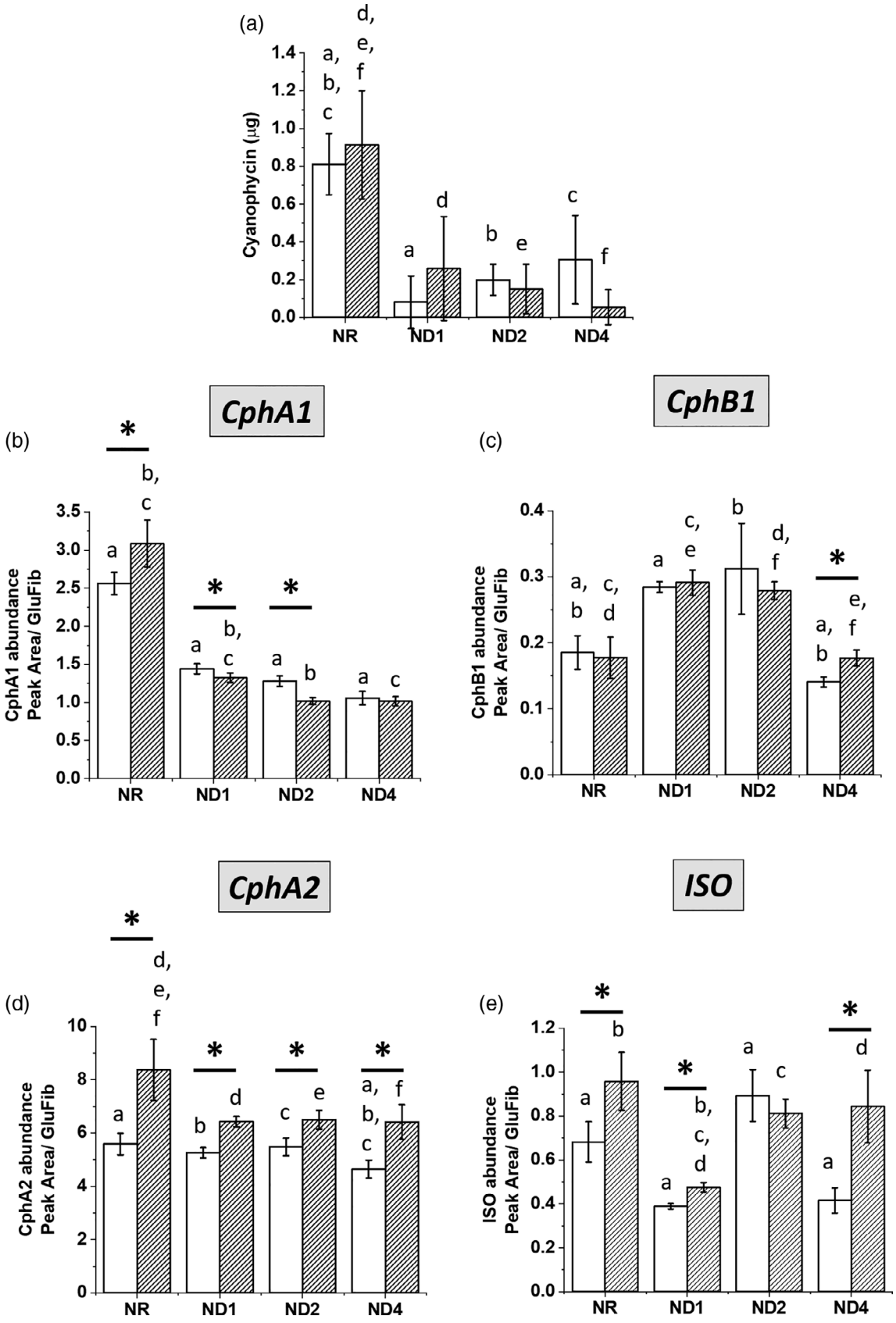

FIGURE 8 Legend on next page.

two strains upon N deprivation (Figure 9A,B), suggesting a comprehensively different regulation of whole central metabolism (Christensen et al., 2019; Nakayasu et al., 2017).

Amino acids are substrates for the synthesis of several molecular players, important for the homeostatic control of the cell. Among them, glutathione (Cameron & Pakrasi, 2010) and ophthalmic acid (Ito, Tokoro, Hori, Hemmi, & Yoshimura, 2018) belong to a robust antioxidant buffering system which plays an important role in protecting against reactive oxygen species (ROS) generated as by-product of photosynthetic metabolism (Narainsamy et al., 2016).

Interestingly, while no major differences between the two strains were observed for ophthalmic acid upon N deprivation, the content of reduced glutathione (GSH) increased in WT (Figure 9C) and it decreased in Δ*amt* (Figure 9D), suggesting the mutant suffers from redox stress upon N deprivation.

2.5 | Gln, Glu and 2-OG pools

The metabolic pool concentration of several key metabolites in N metabolism, Gln, Glu and 2-OG [Figure 1 (Böhme, 1998; Martín-Figueroa et al., 2000; Picossi et al., 2005)], was also affected by the *amt* mutation. The pool of free Glu increased in both strains over the course of the experiment (Figure 10A,B), while the concentration of Gln dropped substantially in the wild-type upon N deprivation (Figure 10A). Interestingly, the concentration of Gln is several-fold lower in Δ*amt* under N replete conditions and also drops upon elimination of assimilable N (Figure 10B). Hence, the Gln/Glu ratio in the mutant is indicative of a partially deprived N metabolic status even in the presence of assimilable N (Figure S7 in Data S1), potentially affecting also the metabolic exchange between the two cell types (no difference in the number of heterocysts was observed between the two strains over the course of the experiment, see Figure S4 in Data S1). It is however worth noting that our data describes the abundance and activity of specific proteins/metabolites and enzymes, respectively, and therefore do not provide information regarding metabolic N flux. In order to investigate the latter, metabolic flux analyses would be needed and in future studies this might enable our hypothesis of a partially deprived N metabolic status in the mutant to be confirmed. Similarly, the mutant also has a slightly lower 2-OG content than the parental strain under NR conditions (Figure 10C), and consequently a higher 2-OG/Gln ratio (Figure S8 in Data S1), in line with the hypothesis that 2-OG is indicative of metabolic N availability (M. I. Muro-Pastor, Reyes, & Florencio, 2001). The difference between the two strains is admittedly small, at only around 18% – but then, the decrease in 2-OG following N deprivation is only about 40%, so even this small decrease could represent a change in N status.

3 | DISCUSSION

Biological systems can be fuelled by multiple N sources, but they are all converted to ammonium/ia before assimilation, as the latter is the most reduced and energetically favourable bioavailable form of N. The translocation of ammonium/ia across biological membranes is therefore expected to play a potential key role in the regulation of N metabolism. Active ammonium/ia translocation [whether it involves the charged or uncharged form is still debated and it is likely to depend on the species in question (Boogerd et al., 2011; Javelle et al., 2007; Ludewig, 2006; Ludewig, Neuhäuser, & Dynowski, 2007; Wang, Orabi, Baday, Bernèche, & Lamoureux, 2012)] across biological membranes is catalysed by AMT transporters, a protein family widely distributed across multiple domains of life (Andrade & Einsle, 2007). AMT transporters are known to be involved in ammonium uptake at low pH (<7), when the equilibrium switches towards the charged form and passive diffusion across biological membranes cannot occur, as reported for non-photosynthetic bacteria [e.g., *Bacillus subtilis* (Detsch & Stülke, 2003)]. These transporters are thought to primarily play a role when the concentration of ammonium is limiting [μM concentration (Paz-Yepes et al., 2007)] and this function is expected to be conserved also in cyanobacteria (Boussiba & Gibson, 1991).

In this work we exploited a KO mutant of the whole *amt* cluster (i.e., *Δamt*) in *Anabaena* sp. PCC 7120 (Paz-Yepes et al., 2008) with the aim to investigate how a N_2-fixing cyanobacterium responds to perturbation of N metabolism at a whole cell level. However, it is worth noting that in our experiments cultivation was done under batch conditions, and only some treatments (nitrogen replete) contained a measurable quantity of ammonium/ia in the initial media, all of which was rapidly assimilated. Thus, for most of the experiment, the only available ammonium/ia in the culture would have been that which we expect to be continuously lost from internally generated metabolism and diffusion of uncharged ammonia into the media. An alternative experimental approach to consider in the future would be to utilize a continuous turbidostat culture with a set concentration of

FIGURE 8 Cyanophycin (CPG) content and abundance of the four major enzymes regulating its metabolism in both WT and Δamt strain. (A). Cyanophycin content in both WT and Δamt strains in the four time points chosen in this experiment, according to Figure 4A. The same amount of biomass was processed in all conditions for both strains (see materials and methods). (B)–(E) Abundance of the four major proteins [i.e., Cyanophycin synthetase (CphA1), Cynaophycinase (CphB1), Cyanophycin synthetase 2 (CphA2) and Isoaspartyl dipeptidase (ISO), respectively for b–e] regulating cyanophycin metabolism in 7120, in the four time points chosen in this experiment (Figure 4A). Data are indicated as average ± *SD* of six biological replicates. Statistically significant differences between WT (white bars) and Δamt (striped bars) are indicated with an asterisk, whilst the same alphabet letter indicates statistically significant differences for the same strain in different growth conditions (one-way ANOVA, *p*-value <.05). See Figure S6 in Data S1 for an overview of CPG metabolism. It is worth noting that Isoaspartyl dipeptidase involved in CPG metabolism has recently been named ladC (Flores, Arévalo, & Burnat, 2019)

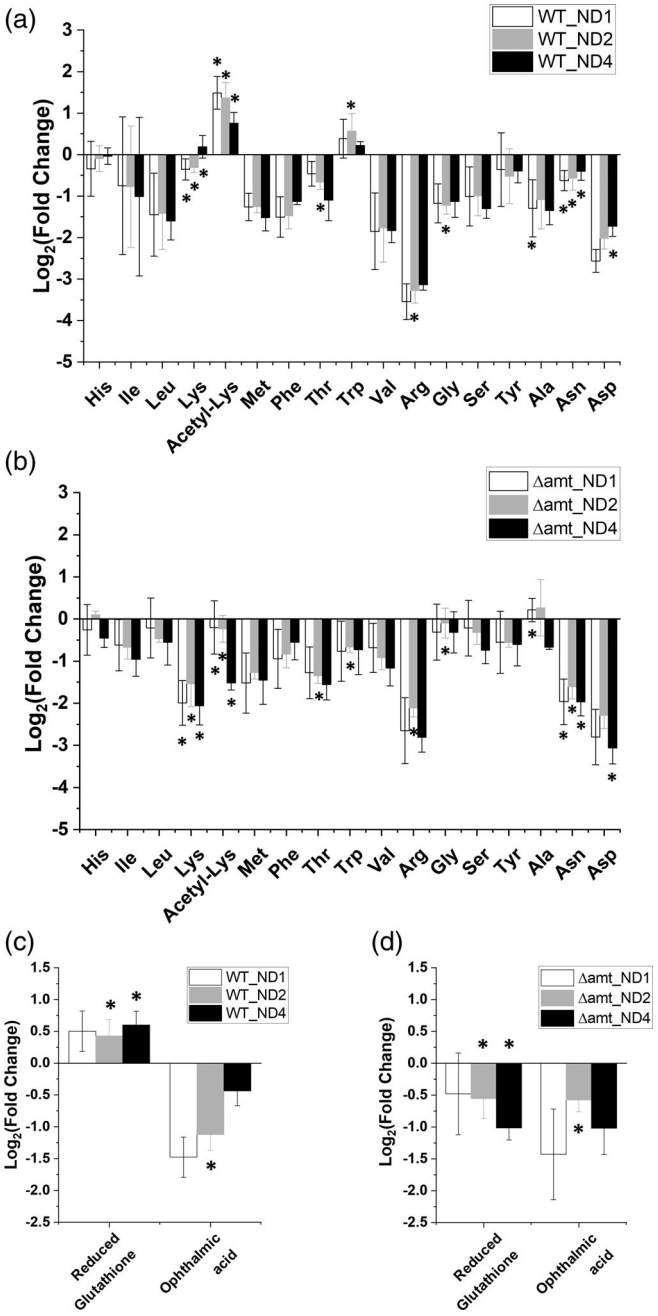

FIGURE 9 Pool of free amino acids and oxidative stress markers in both WT and Δamt strain, upon N deprivation. Free amino acid pool (A and B) and oxidative markers (C and D) in the WT strain (A and C) and in the Δamt mutant (B and D) in the four time points chosen in this experiment, according to Figure 4a. Data are expressed as base two logarithm of the fold change (FC) of the abundance of each metabolite between each of the three time points after N deprivation (i.e., ND1, 2 and 4) and N replete conditions (NR). Data are indicated as average ± *SD* of six biological replicates. Statistically significant differences between WT and Δamt for each metabolite at a specific time point are indicated with an asterisk (one-way ANOVA, *p*-value <.05)

ammonium/ia provided by the media feed. However, that would substantially limit opportunities for the number of replicates and treatments.

We cultivated both 7120 WT and *Δamt* strains in different N regimes (i.e., different N sources and N replete/deplete conditions). The underlying idea was to trigger different inner N states and investigate them through physiological, proteomic and metabolomic analyses. Upon N deprivation, *Anabaena* sp. PCC 7120 differentiates a fraction of its cells into heterocysts to enable efficient N fixation (Golden & Yoon, 1998; Kumar et al., 2010), posing several limitations to integrated studies such as this one. One of them is the need to process the samples as a mixture of the two cell types, in order to avoid metabolic changes that are inevitable consequence of physical separation (Ermakova et al., 2014). This necessary choice forgoes discrimination of the metabolic status of the two cell types. Nevertheless, some proteins and metabolites are unique to one of the two cell types (Martín-Figueroa et al., 2000), enabling to partially overcome such limitations. Moreover, we did not observe any difference in the ratio of heterocysts to vegetative cells in response to any of the genetic or environmental treatments investigated in this work (Figure S4 in Data S1).

3.1 | Lack of AMT transporters triggers a substantial response at the whole cell level, but does not induce any visible phenotypic change

In the constant laboratory conditions tested in this work, we observed AMT transporters are not essential to support growth of 7120, regardless of the N source used to sustain the central metabolism (Figures 2A and 4A), as previously reported in the same organism (Paz-Yepes et al., 2008) and also in *Synechococcus elongatus* (Paz-Yepes et al., 2007). This finding corroborates what has been observed in other bacteria [e.g., *R. capsulatus* (Yakunin & Hallenbeck, 2002)], suggesting an additional conserved transporter-independent function for AMT transporters across unrelated bacteria species.

Nevertheless, the mutant surprisingly displays several changes in the abundance of proteins and metabolite pools with a central role in N metabolism, triggering also a substantial effect on key enzymatic activities. Among them, we observed: (a) a substantial increase in nitrogenase activity (Figures 2B and 5A), likely due to an increased accumulation of the protein complex (Figure 5B,C); (b) an increased GS activity in $NH4^+$-replete conditions and upon prolonged N deprivation (Figures 2C and 6A), as a consequence of changes in the abundance of proteins which play both a direct and/or indirect role on GS activity such as: (a) changes in the abundance of both the GS protein itself (Figures 3A and 6B) and the post-translational negative regulator IF7A (Figure S3 in Data S1 and Figure 6C) and (b) changes in the abundance of GDH, GOGAT and IDH, which re-generate its substrates (Figure S5 in Data S1). It is worth noting that some of these observations correlate with what has already been observed in other organisms, such as the photosynthetic purple bacterium *R. capsulatus*, in which the absence of the AMTB transporter influenced both nitrogenase and GS activity, thus strengthening the hypothesis that such proteins might share the same role in the regulation of N metabolism, even in distinct bacteria species (Yakunin & Hallenbeck, 2002).

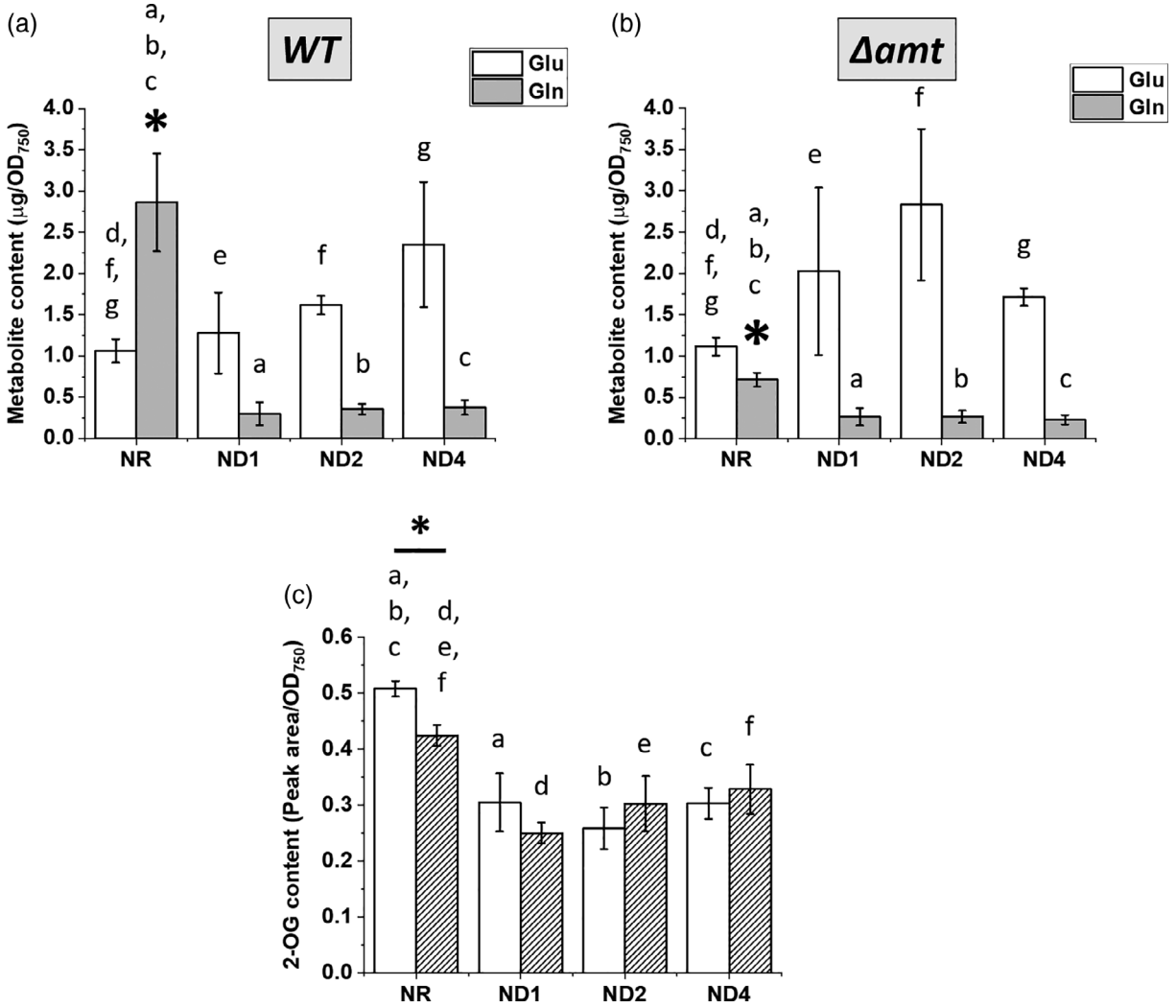

FIGURE 10 Metabolic pool concentration of key metabolites in N metabolism. Glu, Gln (A, B) and 2-OG (C) content in 7120 WT and Δamt strains, in the experimental conditions of Figure 4a. Glu (white bars) and Gln (grey bars) content is split in two distinct panels for WT (A) and Δamt (B). (C) 2-OG content in WT (white bars) and Δamt (striped bars). Results come from the same amount of biomass for both strains and for different growth conditions. Data are indicated as average ± *SD* of six biological replicates. Statistically significant differences between WT and Δamt for each metabolite at a specific time point are indicated with an asterisk, whilst the same alphabet letter indicates statistically significant differences for the same strain and metabolite, in different growth conditions (one-way ANOVA, *p*-value <.05)

Moreover, we also observed that the pool of free amino acids (Figure 9A,B), redox markers (Figure 9C,D) and metabolites with a key role in N metabolism orchestration (i.e., Gln, Glu and 2-OG, Figure 10) is affected by the mutation. The *Δamt* mutant also displays substantial changes in photosynthetic performances and pigment content with respect to the parental strain (Figure 4B and Table 1).

It is worth noting that the biochemical changes observed in the mutant do not translate in any phenotypic difference with respect to the parental strain (i.e., growth is unaffected, Figures 2A and 4A), highlighting the strong robustness of the biological system under investigation. The latter most likely depends on its ability to undergo this very substantial homeostatic adjustment at the whole cell level, as a consequence of both genetic (i.e., *Δamt*) and environmental treatments (i.e., different N regimes).

3.2 | Lack of AMT transporters induces metabolic adaptation spanning both C and N metabolism, with a potential impact on the metabolites exchange between heterocysts and vegetative cells

As in many biological systems, N and C metabolism is expected to be tightly coupled (Zhang et al., 2018) also in 7120, thereby maintaining a properly balanced C/N ratio even when exposed to external perturbations (Forchhammer & Selim, 2019). When the C source (i.e., CO_2 in case of phototrophic metabolism) is not limiting, external N source(s) are expected to directly influence the C/N balance of the cell, with both: (a) efficiency in uptake and (b) abundance and nature of such N source(s) playing a central role. In our experiments, 7120 was cultivated in a 1% CO_2-enriched atmosphere in order to avoid C limitation and both genetic (i.e., *Δamt* mutation) and environmental (i.e., different N

sources and abundance) treatments were used to perturb both such parameters and investigate the response of 7120 at a whole cell level.

The mutant displayed substantial changes in the abundance of several metabolites (Figure 9), including Gln, Glu and 2-OG. Among them, it is worth noting the difference in the free pool of acetyl-lysine (Figure 9A,B) which suggests the overall central metabolism regulation might be comprehensively affected as a consequence of the mutation (Christensen et al., 2019; Nakayasu et al., 2017). The observed differences in the free pool of acetyl-lysine might reflect either changes in total protein acetylation, or else changes in the turnover rates of acetylated proteins, with a potential regulatory role in both photosynthesis and carbon metabolism, as suggested in *Synechocystis* sp. PCC 6803 (Mo et al., 2015). Further confirmation in the lab is however needed to clarify the regulatory role of protein acetylation in 7120.

Differences in the accumulation of Gln, Glu and 2-OG are a clear hallmark of a perturbed C/N balance (Figure 10). Gln, Glu and 2-OG are in fact key metabolites involved in the GS-GOGAT cycle, hence they play a critical role in the central crossroad for C and N metabolism. Moreover, Gln and Glu metabolism is intertwined with that of several other amino acids as they are the most important amino groups donor for their synthesis (Huergo & Dixon, 2015; Reitzer, 2003), while 2-OG is the major signalling metabolite used to perceived the intracellular N status by cyanobacteria (M. I. Muro-Pastor et al., 2001). In our experiments, 2-OG concentration decreased upon N deprivation (Figure 10C) and this correlates with the observed increase in the pool of free Glu (Figure 10A,B), as cyanobacteria lack 2-OG dehydrogenases and therefore 2-OG is mainly used for the biosynthesis of Glu or other Glu-derived compounds (Herrero et al., 2001). It is worth noting that this trend is not affected by the mutation (Figure 10C), which instead induces a reduction in the content of 2-OG in NH_4^+-replete conditions (Figure 10C).

In the literature, the concentration of 2-OG is reported to increase upon nitrogen deprivation (Laurent et al., 2005; M. I. Muro-Pastor et al., 2001). 2-OG lies at the intersection between carbon and nitrogen metabolism, as it is both an intermediate of the tricarboxylic acid (TCA) cycle and provides carbon skeleton to enable assimilation of ammonium/ia in the cell. In several biological systems, fluctuations in the concentration of 2-OG reflect the carbon and nitrogen status of the cell (Huergo & Dixon, 2015). In *Anabaenea* sp. PCC 7120, the concentration of 2-OG increases to promote heterocyst differentiation (Li, Laurent, Konde, Bé du, & Zhang, 2003), upon N deprivation. However, heterocyst differentiation happens within the first 6–8 hr of N deprivation, by the generation of proto-heterocysts that turn into functional heterocysts within 24 hr (Harish & Seth, 2020; A. M. Muro-Pastor & Hess, 2012). It is thus reasonable to expect that the increase in the concentration of 2-OG which triggers heterocyst differentiation occurs mainly within the first few hours upon nitrogen deprivation. Experimental work performed so far in *Anabaenea* sp. PCC 7120 focused mainly/only on the initial few hours (i.e., from few minutes to 2–4 hr) after nitrogen deprivation. This might explain why the concentration of 2-OG has been reported to increase upon nitrogen deprivation (Laurent et al., 2005; M. I. Muro-Pastor et al., 2001). In Laurent et al. (2005), the concentration of 2-OG peaks after 1–2 hr upon removal of combined nitrogen from the cultivation medium and after that the concentration returns to the initial value. Our work differentiates from the available literature as we intentionally designed a longer-term experiment with a first data point collected 24 hr after N deprivation. An increase in the concentration of 2-OG was therefore not observed as we skipped the initial differentiation phase of vegetative cells into heterocysts and the latter, in our first data point, are already fully differentiated (Figure S4 in Data S1). The present study was primarily designed to provide novel information on how this species behaves at a whole-system level upon protracted nitrogen deprivation.

Taken together, our data suggests that the absence of AMT transporters results in a metabolic adjustment in response to environmental treatments (i.e., different N regimes), and although not investigated in the present study, this is likely to affect also the flux of metabolites between heterocysts and vegetative cells, as also suggested by the observed differences in CPG metabolism (Figure 8). The reduction of CPG in the mutant raises the following question: where is the excess N if we have not observed any altered growth phenotype nor a difference in the uptake of N from the external environment? Even if not measured in this work, we hypothesise that any changes in N availability most likely will affect the total protein pool, as it is the major sink for N in *Anabaena* (Simon, 1973). This hypothesis is supported by the general observation that the concentration of most protein targets in the mutant strain increased (e.g., increased accumulation of nitrogenase complex as reported in Figure 5B,C).

3.3 | Are AMT transporters an integral part of the regulatory/signalling network of N metabolism?

In our experiments, we repeatedly observed substantial changes in GS activity, as a consequence of the mutation. The mutant in fact displays an increased GS activity in NH_4^+ replete and also under prolonged N deplete conditions (Figures 2C and 6A), likely in response to changes in the abundance of both the GS protein itself and its post-translational regulator IF7A (Figures 3 and 6). Moreover, we observed that GS activity is often retained even if IF7A abundance varies, potentially suggesting an additional molecular player(s) might also be involved in its regulation. Taken together, our results suggest AMT transporters may play a direct or indirect IF7A-independent role on GS activity in 7120, thus calling for further scientific efforts in order to fill potential gaps in the regulatory/signalling network of N metabolism.

The changes observed in this work are widespread at a whole cell level, also affecting the master molecular players which orchestrate N metabolism (i.e., NtcA, PII and PipX, Figure 7). It is worth noting that the concentration of the three master regulators do not correlate with the observed GS activity (Figure 6A). For example, NtcA is expected to have multiple transcriptional targets (Picossi et al., 2014) which might also inversely control GS activity. Interestingly, the mutant displays an increased abundance of PII in N replete conditions, with respect to the parental strain (Figure 7B). PII belongs to one of the

most widely distributed families of signal transduction proteins in nature, involved in various aspects of N metabolism and regulation of C/N homeostasis (Arcondeguy et al., 2001; Forcada-Nadal, Llácer, Contreras, Marco-Marín, & Rubio, 2018; Forchhammer, 2004, 2008). Among them, in heterotrophic bacteria and in archaea, PII proteins of the subfamily GlnK directly interact with AMT transporters to regulate their activity, typically reducing their uptake rate in N excess conditions to prevent intracellular over-accumulation of ammonium (Arcondeguy et al., 2001). Several studies suggest the PII protein binds AMT transporters also in cyanobacteria [i.e., *Synechocystis* sp. PCC 6803 (Watzer et al., 2019)] and in purple bacteria [e.g., *R. capsulatus* (Tremblay & Hallenbeck, 2008)]. In the latter organism, AMT proteins have been implicated in the posttranslational regulation of nitrogenase, driven by a direct interaction between AMTB and GlnK (a homolog of PII) (Tremblay & Hallenbeck, 2008). Our observation that there is greater PII abundance in the *Δamt* strain supports the hypothesis that PII might retain this function also in 7120. This is one likely explanation for why the disruption of AMT transporters influences the regulatory/signalling network of N metabolism in 7120.

Such a scenario would most likely involve a global mechanism by which 7120 filaments sense nitrogen sufficiency according to the external availability of fixed N. Studies in *Anabaena variabilis* ATCC 29413 suggest that filaments can differentiate between the availability of external and internal N, through a mechanism operating at whole-cellular system level (Thiel & Pratte, 2001). Do AMT transporters belong to such a global sensing mechanism in this species? Further experimental work will be needed to clarify this hypothesis.

We were surprised to find that the molecular fingerprint of *Δamt* cells displays symptoms of N -deficiency relative to the parental strain, also under NH_4^+ replete conditions, and that observations at both the protein and metabolite level support this hypothesis. Among them: (a) the faster activation of nitrogenase upon N deprivation (Figure 5A), (b) the increased GS activity (Figure 6A), (c) the strong reduction in the Gln/Glu ratio (Figure S7 in Data S1), (d) the slightly reduced 2-OG content (Figure 10C) and (e) the increased 2-OG/Gln ratio (Figure S8 in Data S1). A possible explanation is that the mutant experiences a limitation in the free pool of internal ammonium/ia. The latter might explain why the free Gln pool is lower under NR conditions, as the lack of substrate is likely to lower flux through the GS reaction. This might also explain the observed increase in GS activity as a compensatory mechanism. In contrast, in the parental strain, the greater Gln concentration likely drives a Gln-feedback loop, possibly controlled by a homolog of the Gln-sensitive riboswitch recently described in *Synechocystis* sp. PCC 6803 (Klähn et al., 2018). Further work is needed to confirm the existence of a similar molecular mechanism also in 7120.

In contrast to other indicators of N-deficiency, the greater photosynthetic activity (Figure 4B) and Chl/Car ratio (Table 1) suggests the mutant does not suffer from N limitation in NR conditions. This raises the interesting question: what is cause and what is effect? The observed changes at the protein level are coupled to a widespread metabolic adaptation, as a consequence of the mutation, involving substrates and products of most of the enzymatic reactions investigated at the protein level. In fact, it is reasonable to expect that some of the changes in the accumulation of specific proteins might simply result from an adaptation to perturbations of the metabolite pool or *vice versa*. At this point, we thus cannot conclude whether the *Δamt* mutant either is directly suffering from an imbalanced regulatory/signalling network or if it suffers from perturbations at the metabolite level, which are sensed by such regulatory/signalling network. In addition, we cannot conclude whether AMT proteins are only an integral part of the regulatory network, or if they act as a sensor, a regulator, or both, or if they only influence sensing and regulation of N metabolism. Some of the molecular perturbations we observed suggest a possible direct involvement of AMT proteins in the regulation/signalling of N metabolism (i.e., potential direct interaction with the protein PII as discussed above).

A potential role for AMT transporters might be to prevent leakage of ammonium from the nitrogenase reaction under diazotrophic conditions. It should be noted that only a fraction of our experiment (i.e., the first 48 hr) was performed with measurable ammonium in the media, while the majority of the time points were collected in N deprivation (Figure 4A). Therefore, in most of the experiment, the only available ammonium/ia in the culture is expected to be that lost from internally generated metabolism and diffusion of uncharged ammonia into the media.

4 | CONCLUSIONS

We investigated how a mutant of *Anabaena* sp. PCC 7120, missing the whole *amt* cluster, responds to environmental treatments affecting the inner N status of the cells. The whole cell system responds with substantial internal perturbations embracing both N and C metabolisms. Moreover, the absence of AMT transporters leaves a molecular fingerprint suggesting N-deficiency, which does not lead to any externally measurable phenotypic effect. We thus hypothesise that 7120 evolved a robust regulatory/signalling molecular network to maintain N metabolism homeostasis. The observed changes involve both proteins and metabolites, highlighting a pleiotropic effect of the mutation. We also provided evidence of perturbations to nitrogenase and GS activity, as well as to master regulators orchestrating N metabolism, thus leading to the hypothesis that a possible direct or indirect IF7A-independent role of AMT transporters on GS activity exists in 7120, possibly transduced via the PII protein. Taken together, these evidences suggest AMT transporters might play a mechanistic role in the regulatory/signalling network of N metabolism. Nevertheless, it is not possible to exclude that the observed internal changes are just a metabolic adaptation as a consequence of the mutation. In turn this may trigger perturbations at a potential central regulatory/signalling bottleneck controlling the internal supply of ammonium to the cell, for example, through a similar riboswitch mechanism as was reported in *Synechocystis* sp. PCC 6803 (Klähn et al., 2018). Further scientific efforts are needed in order to confirm such a controller also in *Anabaena*. More generally speaking, the work highlights the dynamic and complex nature of internal mechanisms involved in maintaining

homeostasis and the success in so doing, achieving a near-complete lack of any measurable external impact.

5 | MATERIAL AND METHODS

5.1 | Cyanobacteria strains and growth conditions

Strains of *Anabaena* sp. PCC 7120 used in this work are summarized in Table 2 and were kindly provided by Prof. Enrique Flores [institute of Plant Biochemistry and Photosynthesis, University of Sevilla (Sevilla, Spain)].

Both strains were maintained in solid BG11 medium (pH 8.0 with the addition of 10 mM final concentration of TES-NaOH buffer) (Rippka, Deruelles, & Waterbury, 1979) (1.5% Difco Bacto agar, BD) in an Algaetron 230 (PSI, Photon Systems Instruments, Czech Republic), with an atmosphere enriched in CO_2 (1%), under cool white light at 60 μmoles of photons*m^{-2}*s^{-1}, 30°C. Illumination rate was determined using a LI-250A photometer (Heinz-Walz, Effeltrich, Germany). Before starting an experiment, both strains were switched to liquid medium and pre-cultivated axenically in 100-ml Erlenmeyer flasks in 20 ml $BG11_0$ (BG11 medium, without $NaNO_3$) supplemented with 5 mM NH_4Cl in the same growth conditions, under orbital shaking at 160 rpm. Cells were kept in exponential growth conditions, refreshing the cultures every other day (i.e., replacing half of the volume of the culture with fresh $BG11_0$ + 5 mM NH_4Cl). *Anabaena* sp. PCC 7120 Δamt strain was cultivated in presence of 10 μg/ml neomycin (Nm).

For all experiments carried out in this work, strains were cultivated in 6-well polystyrene plates in the same growth conditions indicated above. Cells pre-cultivated in Erlenmeyer flasks were washed twice in the final growth medium, through centrifugation for 10 min, 3,500 *g*, RT. Starting OD_{750} for all growth curves = 0.1.

Growth was monitored through OD_{750} in 96-wells polystyrene plates with a multimode spectrophotometer (Tecan Infinite M200 Pro). Linear correlation between OD_{750} and biomass dry weight was confirmed for both strains and the growth ranges measured in this work. Biomass dry weight was measured gravimetrically as previously reported in Perin et al. (2015). Specific growth rate was calculated by the slope of different growth phases for growth curves plotted in logarithmic scale. Cyanobacteria cultures were also monitored through microscopy analysis. A novel high-throughput heterocyst detection method has also been set up (see Supplementary Materials and Methods and Figure S1 in Data S1).

TABLE 2 Strains of Anabaena sp. PCC 7120 used in this work

Strain	Genotype	Source
Anabaena sp. PCC 7120 WT	Wild-type (WT)	Prof. Enrique Flores
Anabaena sp. PCC 7120 Δamt	Δamt::C.K3; $Amt4^-$, $Amt1^-$, $AmtB^-$, Nm^R	Paz-Yepes et al. (2008)

5.2 | Pigments content and photosynthetic efficiency

Pigments from intact cells grown in 6-wells plates were extracted using a 1:1 biomass to solvent ratio of 100% methanol, at 4°C in the dark for at least 20 min (Sinetova, Červený, Zavřel, & Nedbal, 2012). Absorbance at 470, 665 and 730 nm was monitored using a multimode spectrophotometer (Tecan Infinite M200 Pro) to determine pigment concentrations, using specific extinction coefficients (Ritchie, 2006; Wellburn, 1994).

Photosynthetic efficiency was assessed measuring *in vivo* chlorophyll fluorescence of intact cells using an AquaPen-C AP 110-C (PSI, Photon Systems Instruments, Czech Republic). Photosystem II (PSII) functionality was assessed as PSII maximum quantum yield (Φ_{PSII}), according to Maxwell and Johnson (2000)).

5.3 | Ammonium/ia quantification

Ammonium/ia quantification was performed using an adaptation of the method described by Willis, Montgomery, and Allen (1996)) in order to enable the use of 96-well microtiter plates. Briefly, *Anabaena* sp. PCC 7120 strains grown in 6-well plates were harvested by centrifugation and 10 μl of the cell-free supernatant were loaded in a flat-bottom 96-well plate. 200 μl of reactive solution (32 g/L sodium salicylate, 40 g/L $Na_3PO_4{\cdot}12H_2O$ and 0.5 g/L sodium nitroprusside) and 50 μl of hypochlorite solution (0.25–0.37% active chlorine) were added in this order to the cell-free sample and the solution made homogenous, before measuring the absorbance at 685 nm in a multimode spectrophotometer (Tecan Infinite M200 Pro), after incubation for 15 min, 900 rpm, RT in a shaker (PHMP, Grant Instruments). Ammonium/ia concentration in the cell-free samples was calculated using the linear range of a standard curve prepared with serial dilutions of a NH_4Cl solution.

5.4 | Enzymatic activities

5.4.1 | Glutamine synthetase

Glutamine synthetase (GS) activity was assessed through the method detailed below, which comes from the combination of different protocols from (Bressler & Ahmed, 1984; Merida, Candau, & Florencio, 1991; Orr et al., 1981).

5.4.1.1 Preparation of cell-free total proteins extracts

Strains of *Anabaena* sp. PCC 7120 grown in 6-wells plates were harvested by centrifugation and the supernatant discarded. Cell pellets were transferred to 2 ml polypropylene tubes and disrupted twice using a TissueLyser II (Qiagen), adding the same volume of acid-washed glass beads (Sigma-Aldrich) and solubilisation buffer (50 mM Hepes, 0.2 mM EDTA, pH 7.3), for 5 min at 30 Hz. Tube holders were pre-cooled at

−20°C. Cell extracts were collected through centrifugation for 10 s, 9000 *g*, 4°C. Cell extracts were centrifuged twice for 10 min, 21,000 *g*, 4°C to eliminate cell debris and insoluble proteins. Total proteins concentration in the cell-free lysate was assessed through DC protein assay (BIO RAD), following the manufacturer's manual, using 96-wells plates against a BSA (bovine serum albumin) standard curve.

5.4.1.2 GS activity assay

GS catalyses the condensation of glutamate and ammonia to generate glutamine, hydrolysing ATP:

$$Glutamate + NH_3 + ATP \rightarrow Glutamine + ADP + P$$

GS activity can be measured indirectly, quantifying the amount of phosphate released by the reaction through colorimetric assay.

Enzymatic assay was performed in 550 µl in 24-wells flat bottom polystyrene plates, with 50 µg total proteins in 364 mM imidazole-HCl, pH 7.0, 1.82 mM NH_4Cl, 5.45 mM Na-ATP·H_2O, pH 7.0 (prepared fresh on ice), 0.52 M $MgCl_2 \cdot 6H_2O$, 91 mM sodium glutamate, pH 7.0, for 15 min, 400 rpm, 30°C in a thermoshaker (PHMP, Grant Instruments). The reaction was then quenched on ice, adding $FeSO_4 \cdot 6H_2O$ (0.61% w/v in 0.011 N H_2SO_4 final concentration). In order to develop colour (proportional to the amount of phosphate released by ATP as a consequence of GS activity), ammonium heptamolybdate (0.4% w/v in 0.45 M H_2SO_4 final concentration) was added to the reaction and solutions were homogenised on ice. Colour intensity of clear samples was measured at 850 nm, using a multimode spectrophotometer (Tecan Infinite M200 Pro). GS activity was calculated subtracting to each sample the OD_{850} of the corresponding blank solution (prepared replacing the substrate sodium glutamate with water and corresponding to the background signal of phosphate released by other endogenous ATP-dependent enzymatic reactions).

5.4.2 | Nitrogenase

Nitrogenase activity was determined with an acetylene reduction assay under oxic culture conditions. Cells grown in 6-well plates were incubated in 2-ml gas chromatography glass vials under an atmosphere of 10% acetylene in air. Vials were incubated for 3 hr in the same original growth conditions (i.e., shaking, light, 30°C) and the quantity of ethylene in the headspace was determined by gas chromatography (7820A GC system, Agilent Technologies). The nitrogenase activity is expressed as % conversion of added acetylene into ethylene, per hour and per µg of Chl.

5.5 | Cyanophycin content

5.5.1 | Cyanophycin extraction

The same amount of biomass (OD_{750} = 0.3) of different *Anabaena* sp. PCC 7120 strains grown in 6-wells plates was harvested by centrifugation and the supernatant discarded. Cyanophycin was extracted from the cell pellets following the protocol detailed in (Watzer et al., 2015), with some modifications as follows. Briefly, cell pellet was resuspended in 1 ml 100% acetone and incubated in a shaker for 30 min, 1,400 rpm, RT. Lysed cells were then centrifuged for 17 min, 21,000 *g*, RT and the supernatant discarded. Pellet was resuspended in 1.5 ml of 0.1 M HCl and incubated for 1 hr, 1,400 rpm, 60°C to solubilise cyanophycin polymers. Solubilised cyanophycin was centrifuged for 17 min, 21,000 *g*, RT to remove immiscible debris. Tris–HCl, pH 8.0 was added to the supernatant (0.2 M final concentration) and samples incubated for 40 min, 4°C. Samples were then centrifuged for 17 min, 21,000 *g*, 4°C and pelleted cyanophycin polymers were resuspended in 500 µl 0.01 M HCl for quantification.

5.5.2 | Cyanophycin quantification

Cyanophycin is a polymer of arginine and aspartate (Forchhammer & Watzer, 2016) and the quantification of arginine released by cyanophycin granules can be used as proxy for cyanophycin content determination (Burnat et al., 2014). Arginine quantification was performed through a modified colorimetric Sakaguchi method, according to (Messineo, 1966).

5.6 | Proteomic analysis

5.6.1 | Sample preparation

Strains of *Anabaena* sp. PCC 7120 grown in 6-wells plates were harvested by centrifugation and the supernatant discarded. Cell pellets were transferred to 2 ml polypropylene tubes and disrupted using a TissueLyser II (Qiagen), adding the same volume of acid-washed glass beads (Sigma-Aldrich) and extraction buffer (20 mM Tris–HCl, pH 8.0, 1 mM EDTA, pH 8.0 and 2 mM DTT), for 5 min at 30 Hz. Tube holders were pre-cooled at −20°C. Cells disruption was repeated twice and cell extracts were collected through centrifugation for 10 s, 9,000 *g*, 4°C and pulled together after both cycles. Cell extracts were centrifuged twice for 10 min, 21,000 *g*, 4°C to eliminate cell debris and insoluble proteins. Total proteins concentration was assessed through DC protein assay (BIO RAD), following the manufacturer's manual, using 96-wells plates against a BSA (bovine serum albumin) standard curve. Cell extracts were diluted by 0.1 M ammonium bicarbonate to have a 0.3 µg/µl total proteins final concentration and the standard peptide [Glu1]-Fibrinopeptide B, human (GluFib, Sigma Aldrich) was added (0.3 ng/µl, final concentration). Samples were reduced by DTT and ammonium bicarbonate (final concentration 10 mM and 50 mM, respectively) for 1 hr, 56°C, and subsequently alkylated adding iodoacetamide prepared fresh in 0.1 M ammonium bicarbonate (50 mM final concentration), for 30 min, 37°C, 500 rpm in a thermoshaker (PHMT; Grant Instruments). Alkylated samples were digested by proteomics-grade trypsin (Promega), final concentration 6 ng/µl, ON, 37°C. Tryptic digestion was stopped quenching the reaction with formic acid (final concentration 1%) for 30 min, 37°C,

500 rpm in a thermoshaker. Acidified samples were centrifuged at 17,000 *g*, RT, to pellet water immiscible degradation products and the supernatant collected for mass spectrometry analysis.

5.6.2 | Mass spectrometry

Trypsin digested samples were analysed on an AB-SCIEX 6500QTrap MS coupled to an Agilent 1,100 LC system. Chromatography was performed on a Phenomenex Luna C18(2) column (100 mm × 2 mm × 3 μm) at 50°C, using a gradient system of solvents A (94.9% H_2O, 5% CH_3CN and 0.1% formic acid) and B (94.9% CH_3CN, 5% H_2O and 0.1% formic acid). A gradient from 0 to 35% B over 30 min at a flow rate of 250 ml/min was used. The column was then washed with 100% B for 3 min and then re-equilibrated with 100% A for 6 min. Typically 40 μl injections were used for the analysis. The MS was configured with an Ion Drive Turbo V source; Gases 1 and 2 were set to 40 and 60, respectively; the source temperature to 500°C and the ion spray voltage to 5,500 V. MS, configured with high mass enabled, was used in "Trap" mode to acquire Enhanced Product Ion (EPI) scans for peptide sequencing and in "Triple Quadrupole" mode for Multiple Reaction Monitoring (MRM). Data acquisition and analysis was performed with SCIEX software Analyst 1.6.1 and MultiQuant 3.0. Signature peptides for all the proteins investigated in this work were determined through trial MRM runs. Only the peptide GluFib was used as standard for protein normalization. The typical work-flow to select the best signature peptides involved the analysis of trial samples in different growth conditions using transitions generated by *in silico* analysis with the open-source Skyline Targeted Mass Spec Environment (MacCoss Lab) (Abbatiello et al., 2013; MacLean et al., 2010). The identity of candidate peptides was then confirmed by EPI scans. Background proteome of *Anabaena* sp. PCC 7120 (http://genome.kazusa.or.jp/cyanobase) was used to check for uniqueness of target peptides. Typically, 3–5 transitions per peptide were used. The final method includes 1–4 peptides per protein for unique identification and quantification. Signature peptides for all the proteins investigated in this work are listed in Table 3.

Protein quantification was performed accounting for the intensities of all transitions peaks for all the peptides belonging to a specific protein. The resulted peak area was normalized to the peak intensity of the GluFib peptide standard.

5.7 | Metabolomic analysis

5.7.1 | Sample preparation

Strains of *Anabaena* sp. PCC 7120 grown in 6-wells plates were harvested by fast filtration, modifying the protocol from (Eisenhut et al., 2008). Briefly, cells were fast filtered in the light without any subsequent washing step, using a vacuum filtration system (0.45 μm pore size nitrocellulose filter, 47 mm diameter [Sigma Aldrich]), using stainless-steel stand and funnel (Sartorius). Filters were then transferred to 50 ml tubes and immediately frozen in liquid nitrogen and stored at −80°C until metabolites extraction. Time between harvesting and metabolic inactivation by freezing was <10 sec. Deep frozen cells were scraped off the nitrocellulose filters using 80% cold methanol (−20°C). Cells in cold methanol were transferred to 2 ml polypropylene tubes and metabolite extraction was carried out with a TissueLyser II (Qiagen), using tube holders pre-cooled at −20°C and adding the same volume of acid-washed glass beads (Sigma-Aldrich), for 5 min at 30 Hz. Metabolites were collected after centrifugation for 10 min, 21,000 *g*, 4°C. Metabolite extraction was repeated twice, the extracts pooled together and centrifuged again to separate cell debris and other immiscible products. Metabolic extracts were then dried by vacuum centrifugation overnight and stored at −80°C until use.

5.7.2 | Sample derivatization and mass spectrometry

Dried metabolic extracts were reconstituted in 300 μl of water, using L-phenylalanine-d_5 as internal standard (final concentration 2 μg/ml), then vortexed and centrifuged at 16,000 *g* for 10 min. Quality control (QC) samples were prepared by mixing 10 μl of the supernatant of each sample, with the analytical batch including 10% QC samples.

5.7.2.1 Amino acids quantification

6-aminoquinolyl-N-hydroxysuccinimidyl carbamate was used for derivatization (AccQTag derivatization) according to the manufacturer's manual (AccQTag, Waters Corp). Briefly, 70 μl of borate buffer (pH 8.6) was added to 10 μl sample, followed by the addition of 20 μl AccQTag reagent (in acetonitrile). Samples were then vortexed and heated at 55°C for 10 min. 5 μl of each sample were analysed by HPLC-electrospray ionisation/MS–MS using a Shimadzu UFLC XR/AB SCIEX Triple Quad 5,500 system, running in multiple reaction monitoring (MRM) via positive ionization mode. The LC–MS method here exploited is based on the one previously described by Gray et al. (2017)), with some modifications, as detailed below.

5.7.2.2 LC method

Mobile phase A: LC–MS grade water with 0.5% formic acid; mobile phase B: LC–MS grade acetonitrile with 0.5% formic acid. Flow rate: 300 μl/min, with the following gradient elution profile: 0.1 min, 4% B; 10 min, 28% B; 10.5 min, 80% B; 11.5 min, 80% B; 12 min, 4% B; 13 min,4% B. An Acquity HSS T3 UPLC column [2.1 mm × 100 mm, 1.8 μm particle size (Waters Corporation, Milford, MA, U.S.A.)] was used to achieve metabolite separation at 45°C.

5.7.2.3 MS method

The data were acquired through a Sciex QTRAP 5500 MS/MS system [Applied Biosystem (Forster City, CA, USA)], using the following settings: curtain gas, 40 psi; collision gas, medium; ionspray voltage, 5,500 V; temperature, 550°C; ion source gas 1 and 2, 40 and 60 psi, respectively. De-clustering, entrance and collision cell exit potentials

TABLE 3 Signature peptides for the proteins investigated in this work

Gene ID	Protein ID	Biological function	Peptides sequence
Alr1827	**IDH**	Isocitrate dehydrogenase	K.GPLTTPVGGGIR.S [100, 111]
			R.SLNVALR.Q [112, 118]
			K.LDVIVYR.E [146, 152]
Alr2328	**GS**	Glutamine synthetase	K.IELIDLK.F [15, 21]
			K.LGVPIEK.H [205, 211]
			R.IPLSGTNPK.A [348, 356]
			K.NIYELSPEELAK.V [399, 410]
Alr4344	**GOGAT**	Glutamine oxoglutarate aminotransferase	R.FAQVTNPAIDPLR.E [548, 560]
			R.SLSEIIGR.A [1232, 1239]
			K.TLPIVNTDR.T [1310, 1318]
Alr4255	**GDH**	Glutamate dehydrogenase	R.LDNGDIR.V [66, 72]
			R.TLEGVK.V [227, 232]
Asl2329	**IF7A**	Glutamine synthetase regulator	SAQELGLPAEELSHYWNPTQGK [29, 50]
Alr4392	**NtcA**	Nitrogen-responsive regulatory protein	K.TIFFPGDPAER.V [32, 42]
			R.ENSVFGVLSLLTGNK.S [70, 84]
			R.LLGDLR.E [192, 197]
Ar0485	**PipX**	PII interacting protein	R.LFFLVGNDIK.A [38, 47]
			K.FQPIGR.T [51, 56]
All2319	**PII**	Nitrogen regulatory protein PII	K.IIAAAR.T [76, 81]
			R.TGEIGDGK.I [82, 89]
			K.IFISPVEQVIR.I [90, 100]
All1440	**NifK**	Nitrogenase molybdenum-iron protein beta chain	R.EALTVNPAK.G [59, 67]
			K.AIPEELEIER.G [334, 343]
			R.IGYPLFDR.H [457, 464]
All1554	**NifD**	Nitrogenase molybdenum-iron protein alpha chain	K.ELIQEVLK.A [14, 21]
			K.LIEELDVLFPLNR.G [135, 147]
			K.IAASLR.E [311, 316]
All3879	**CphA1**	Cyanophycin synthetase	K.AELEQDIQDLK.D [144, 154]
			R.GITIDIR.S [269, 275]
			R.GSASELITK.G [808, 816]
All3880	**CphB1**	Cyanophycinase	R.TPQATK.T [23, 28]
			K.VEILDIR.E [90, 96]
			R.DGWLQVLGK.G [232, 240]
Alr0573	**CphA2**	Cyanophycin synthetase 2	K.GIGVTADVK.D [263, 271]
			R.DAVFVNR.S [521, 527]
			R.DDYNSNIQSLLR.N [534, 545]
All3922	**ISO**	Isoaspartyl dipeptidase	R.FSGVINVSR.V [93, 101]
			R.GTIGVVALDTYGK.L [178, 190]
			K.LAVGTSTGGK.G [191, 200]
Standard	**GluFib**	[Glu1]-Fibrinopeptide B, human	EGVNDNEEGFFSAR [0, 13]

Note: Gene ID, protein ID and corresponding biological function are indicated. Peptides sequences show their position within the corresponding protein in square brackets.

were set to 30, 10 and 10 V, respectively. Multiple reaction monitoring (MRM) transitions, retention time (RT) and individually optimized collision energy (CE) for each metabolite are listed in Table S2 in Data S1.

5.7.2.4 2-oxoglutarate (2-OG) quantification

The ion pairing LC method here exploited was adapted from Michopoulos (2018), according to the following settings. Mobile phase A: 10 mM tributylamine (TBA) and 15 mM acetic acid in LC–MS grade

water; mobile phase B: 80% methanol and 20% isopropanol. Flow rate: 400 µl/min, with the following gradient elution profile: 0 min, 0% B; 0.5 min, 0% B; 4 min, 5% B; 6 min, 5% B; 6.5 min, 20% B; 8.5 min, 20% B; 14 min, 55% B; 15 min, 100% B; 17 min, 100% B; 18 min, 0% B; 21 min 0% B. The method was transferred to XEVO TQ-S (Waters, Wilmslow, U.K.), using an Acquity UPLC system with 45°C separation temperature.

MS data were acquired according to the following parameters: capillary voltage, 0.8 kV; source offset, 50 V; desolvation temperature, 500°C; source temperature, 150°C; desolvation gas flow, 1,000 L/h; cone gas flow, 150 L/h; neutralizer gas, 7.0 bar; collision gas, 0.15 ml/min; cone voltage, 80 V. Data were acquired through an electrospray negative ionisation, focusing only on $[M-H]^-$ ions. Retention time (RT), multiple reaction monitoring (MRM) transitions and individually optimised collision energy (CE) are listed in Table S3 in Data S1.

5.7.2.5 Data processing

The raw LC–MS data were analysed using Skyline [MacCoss Lab (K. J. Adams et al., 2020)]. External dilution curves were used to determine the range for linear response.

5.7.2.6 Chemicals and reagents

Metabolite standards (Mass Spectrometry Metabolite Library of Standards, MSMLS) were purchased from IROA Technologies (Michigan, MI, U.S.A.). Acetic acid, tributylamine (TBA), L-phenyl-d5-alanine, were obtained from Sigma-Aldrich (Gillingham, U.K.). LC–MS grade water, water with 0.1% formic acid (v/v) and acetonitrile with 0.1% formic acid (v/v) were purchased from Fisher Scientific (Leicester, U.K.). Methanol and isopropanol were purchased from Honeywell (Charlotte, NC, U.S.A.). AccQTag Ultra reagent was purchased from Waters UK.

5.8 | Statistical analysis

Descriptive statistical analysis was applied for all the data presented in this work. The mathematical correlation between GS activity and IF7A abundance was assessed through Pearson correlation in Microsoft Excel. Statistical significance was assessed by one-way analysis of variance (One-way ANOVA) and Student's *t* test using OriginPro 2018b (v. 9.55) (http://www.originlab.com/). Samples size was at least >4 for all the measurements collected in this work.

ACKNOWLEDGMENTS

We acknowledge professor Enrique Flores from the institute of Plant Biochemistry and Photosynthesis, University of Sevilla (Sevilla, Spain), for kindly providing both the *Anabaena* sp. PCC 7120 wild-type (WT) and the KO strain for the *amt* gene cluster. We also acknowledge help and support from Dr. Mark Bennett and Dr. Paul Hitchen with MRM-MS protein quantification, and from Dr. David Malatinszky for setting up high-throughput GS and ammonium quantification assays. We thank Stephen Rothery (FILM) for help with image analysis and also acknowledge the funding from the Wellcome Trust (grant 104931/Z/14/Z) and BBSRC (grant BB/L015129/1 and BB/N003608/1) which support the Facility for Imaging by Light Microscopy (FILM) at Imperial College London.

CONFLICT OF INTEREST

Authors declare no conflict of interest.

AUTHOR CONTRIBUTIONS

Giorgio Perin and Patrik R. Jones: Conception, design and writing of the manuscript. **Giorgio Perin:** Experiments coordination, sample collection, data collection and analysis. **Tyler Fletcher:** Set up the method for MRM protein quantification and sample run. **Virag Sagi-Kiss:** Set up the method for metabolomic analysis and sample run. **David C. A. Gaboriau:** Set up ImageJ macro for microscope analysis. **Mathew R. Carey:** Sample preparation for metabolomic analysis. **Jacob G. Bundy:** Metabolomic analysis coordination. All authors revised the manuscript and approved its final version.

DATA AVAILABILITY STATEMENT

The data that support the findings of this study are available from the corresponding author upon reasonable request.

ORCID

Giorgio Perin https://orcid.org/0000-0002-9204-4080
Jacob G. Bundy https://orcid.org/0000-0002-1164-8465
Patrik R. Jones https://orcid.org/0000-0001-7618-8204

REFERENCES

Abbatiello, S. E., Mani, D. R., Schilling, B., MacLean, B., Zimmerman, L. J., Feng, X., … Carr, S. A. (2013). Design, implementation and multisite evaluation of a system suitability protocol for the quantitative assessment of instrument performance in liquid chromatography-multiple reaction monitoring-MS (LC-MRM-MS). *Molecular and Cellular Proteomics*, *12*, 2623–2639.

Adams, D. G., Bergman, B., Nierzwicki-Bauer, S. A., Duggan, P. S., Rai, A. N., & Schüßler, A. (2013). Cyanobacterial-plant symbioses. In *The prokaryotes: Prokaryotic biology and symbiotic associations* (pp. 359–400). Berlin Heidelberg: Springer-Verlag.

Adams, D. G., & Duggan, P. S. (2008). Cyanobacteria-bryophyte symbioses. *Journal of Experimental Botany*, *59*, 1047–1058.

Adams, K. J., Pratt, B., Bose, N., Dubois, L. G., St. John-Williams, L., Perrott, K. M., … Thompson, J. W. (2020). Skyline for small molecules: A unifying software package for quantitative metabolomics. *Journal of Proteome Research*, *19*, 1447–1458.

Andrade, S. L. A., & Einsle, O. (2007). The Amt/Mep/Rh family of ammonium transport proteins (Review). *Molecular Membrane Biology*, *24*, 357–365.

Arcondeguy, T., Jack, R., & Merrick, M. (2001). PII signal transduction proteins, pivotal players in microbial nitrogen control. *Microbiology and Molecular Biology Reviews*, *65*, 80–105.

Backer, R., Rokem, J. S., Ilangumaran, G., Lamont, J., Praslickova, D., Ricci, E., … Smith, D. L. (2018). Plant growth-promoting rhizobacteria: Context, mechanisms of action, and roadmap to commercialization of biostimulants for sustainable agriculture. *Frontiers in Plant Science*, *871*(9), 1473.

Bird, C., & Wyman, M. (2003). Nitrate/nitrite assimilation system of the marine picoplanktonic cyanobacterium *Synechococcus* sp. strain WH 8103: Effect of nitrogen source and availability on gene expression. *Applied and Environmental Microbiology*, *69*, 7009–7018.

Böhme, H. (1998). Regulation of nitrogen fixation in heterocyst-forming cyanobacteria. *Trends in Plant Science*, *3*, 346–351.

Bolay, P., Muro-Pastor, M. I., Florencio, F. J., & Klähn, S. (2018). The distinctive regulation of cyanobacterial glutamine synthetase. *Life*, *8*(4), 52.

Boogerd, F. C., Ma, H., Bruggeman, F. J., Van Heeswijk, W. C., García-Contreras, R., Molenaar, D., … Westerhoff, H. V. (2011). AmtB-mediated NH3 transport in prokaryotes must be active and as a consequence regulation of transport by GlnK is mandatory to limit futile cycling of NH_4^+/NH_3. *FEBS Letters*, *585*, 23–28.

Boussiba, S., & Gibson, J. (1991). Ammonia translocation in cyanobacteria. *FEMS Microbiology Letters*, *88*, 1–14.

Bressler, S. L., & Ahmed, S. I. (1984). Detection of glutamine synthetase activity in marine phytoplankton: Optimization of the biosynthetic assay. *Marine Ecology Progress Series*, *14*, 207–217.

Burnat, M., Herrero, A., & Flores, E. (2014). Compartmentalized cyanophycin metabolism in the diazotrophic filaments of a heterocystforming cyanobacterium. *Proceedings of the National Academy of Sciences of the United States of America*, *111*, 3823–3828.

Cameron, J. C., & Pakrasi, H. B. (2010). Essential role of glutathione in acclimation to environmental and redox perturbations in the cyanobacterium *Synechocystis* sp. PCC 6803. *Plant Physiology*, *154*, 1672–1685.

Cardona, T., & Magnuson, A. (2010). Excitation energy transfer to Photosystem I in filaments and heterocysts of *Nostoc punctiforme*. *Biochimica et Biophysica Acta - Bioenergetics*, *1797*, 425–433.

Christensen, D. G., Xie, X., Basisty, N., Byrnes, J., McSweeney, S., Schilling, B., & Wolfe, A. J. (2019). Post-translational Protein Acetylation: An elegant mechanism for bacteria to dynamically regulate metabolic functions. *Frontiers in Microbiology*, *10*, 1604.

Cumino, A. C., Marcozzi, C., Barreiro, R., & Salerno, G. L. (2007). Carbon cycling in *Anabaena* sp. PCC 7120. Sucrose synthesis in the heterocysts and possible role in nitrogen fixation. *Plant Physiology*, *143*, 1385–1397.

Detsch, C., & Stülke, J. (2003). Ammonium utilization in *Bacillus subtilis*: Transport and regulatory functions of NrgA and NrgB. *Microbiology*, *149*, 3289–3297.

Eisenhut, M., Huege, J., Schwarz, D., Bauwe, H., Kopka, J., & Hagemann, M. (2008). Metabolome phenotyping of inorganic carbon limitation in cells of the wild type and photorespiratory mutants of the cyanobacterium *Synechocystis* sp. strain PCC 6803. *Plant Physiology*, *148*, 2109–2120.

Ermakova, M., Battchikova, N., Richaud, P., Leino, H., Kosourov, S., Isojaŕvi, J., … Aro, E. M. (2014). Heterocyst-specific flavodiiron protein Flv3B enables oxic diazotrophic growth of the filamentous cyanobacterium *Anabaena* sp. PCC 7120. *Proceedings of the National Academy of Sciences of the United States of America*, *111*, 11205–11210.

Flores, E., Arévalo, S., & Burnat, M. (2019). Cyanophycin and arginine metabolism in cyanobacteria. *Algal Research*, *42*, 101577.

Flores, E., & Herrero, A. (2005). Nitrogen assimilation and nitrogen control in cyanobacteria. *Biochemical Society Transactions.*, *33*, 164–167.

Forcada-Nadal, A., Llácer, J. L., Contreras, A., Marco-Marín, C., & Rubio, V. (2018). The P_{II}-NAGK-PipX-NtcA regulatory axis of cyanobacteria: A tale of changing partners, allosteric effectors and non-covalent interactions. *Frontiers in Molecular Biosciences*, *5*, 91.

Forchhammer, K. (2004). Global carbon/nitrogen control by PII signal transduction in cyanobacteria: From signals to targets. *FEMS Microbiology Reviews*, *28*, 319–333.

Forchhammer, K. (2008). PII signal transducers: Novel functional and structural insights. *Trends in Microbiology*, *16*, 65–72.

Forchhammer, K., & Selim, K. A. (2019). Carbon/Nitrogen homeostasis control in cyanobacteria. *FEMS Microbiology Reviews*, *44*(1), 33–53.

Forchhammer, K., & Watzer, B. (2016). Closing a gap in cyanophycin metabolism. *Microbiology (United Kingdom)*, *162*, 727–729.

Galmozzi, C. V., Saelices, L., Florencio, F. J., & Muro-Pastor, M. I. (2010). Posttranscriptional regulation of glutamine synthetase in the filamentous cyanobacterium *Anabaena* sp. PCC 7120: Differential expression between vegetative cells and heterocysts. *Journal of Bacteriology*, *192*, 4701–4711.

Golden, J. W., & Yoon, H. S. (1998). Heterocyst formation in *Anabaena*. *Current Opinion in Microbiology*, *1*, 623–629.

Gray, N., Zia, R., King, A., Patel, V. C., Wendon, J., McPhail, M. J. W., … Nicholson, J. K. (2017). High-speed quantitative UPLC-MS analysis of multiple amines in human plasma and serum via precolumn derivatization with 6-aminoquinolyl-*N*-hydroxysuccinimidyl carbamate: Application to acetaminophen-induced liver failure. *Analytical Chemistry*, *89*, 2478–2487.

Harish, & Seth, K. (2020). Molecular circuit of heterocyst differentiation in cyanobacteria. *Journal of Basic Microbiology*, *60*, 738–745.

Herrero, A., Muro-Pastor, A. M., & Flores, E. (2001). Nitrogen control in cyanobacteria. *Journal of Bacteriology*, *183*, 411–425.

Herrero, A., Stavans, J., & Flores, E. (2016). The multicellular nature of filamentous heterocyst-forming cyanobacteria. *FEMS Microbiology Reviews*, *40*, 831–854.

Huergo, L. F., & Dixon, R. (2015). The emergence of 2-Oxoglutarate as a master regulator metabolite. *Microbiology and Molecular Biology Reviews*, *79*, 419–435.

Inomura, K., Bragg, J., & Follows, M. J. (2017). A quantitative analysis of the direct and indirect costs of nitrogen fixation: A model based on *Azotobacter vinelandii*. *ISME Journal*, *11*, 166–175.

Ito, T., Tokoro, M., Hori, R., Hemmi, H., & Yoshimura, T. (2018). Production of ophthalmic acid using engineered *Escherichia coli*. *Applied and Environmental Microbiology*, *84*, e02806–17.

Javelle, A., Lupo, D., Li, X. D., Merrick, M., Chami, M., Ripoche, P., & Winkler, F. K. (2007). Structural and mechanistic aspects of Amt/Rh proteins. *Journal of Structural Biology*, *158*, 472–481.

Kellar, P. E., & Goldman, C. R. (1979). A comparative study of nitrogen fixation by the *Anabaena-Azolla* symbiosis and free-living populations of *Anabaena* spp. in Lake Ngahawa, New Zealand. *Oecologia*, *43*, 269–281.

Klähn, S., Bolay, P., Wright, P. R., Atilho, R. M., Brewer, K. I., Hagemann, M., … Hess, W. R. (2018). A glutamine riboswitch is a key element for the regulation of glutamine synthetase in cyanobacteria. *Nucleic Acids Research*, *46*, 10082–10094.

Kumar, K., Mella-Herrera, R. A., & Golden, J. W. (2010). Cyanobacterial heterocysts. *Cold Spring Harbor Perspectives in Biology*, *2*(4), a000315.

Laurent, S., Chen, H., Bédu, S., Ziarelli, F., Peng, L., & Zhang, C. C. (2005). Nonmetabolizable analogue of 2-oxoglutarate elicits heterocyst differentiation under repressive conditions in *Anabaena* sp. PCC 7120. *Proceedings of the National Academy of Sciences of the United States of America*, *102*, 9907–9912.

Lechno-Yossef, S., & Nierzwicki-Bauer, S. A. (2005). *Azolla-Anabaena* symbiosis. In A. N. Rai, B. Bergman & U. Rasmussen (eds.). *Cyanobacteria in symbiosis* (pp. 153–178). Dordrecht: Kluwer Academic Publishers.

Li J.-H., Laurent S., Konde V., Bé du S., Zhang C.-C. (2003) An increase in the level of 2-oxoglutarate promotes heterocyst development in the cyanobacterium *Anabaena* sp. strain PCC 7120.

Ludewig, U. (2006). Ion transport versus gas conduction: Function of AMT/Rh-type proteins. *Transfusion Clinique et Biologique*, *13*, 111–116.

Ludewig, U., Neuhäuser, B., & Dynowski, M. (2007). Molecular mechanisms of ammonium transport and accumulation in plants. *FEBS Letters*, *581*, 2301–2308.

MacLean, B., Tomazela, D. M., Abbatiello, S. E., Zhang, S., Whiteaker, J. R., Paulovich, A. G., … MacCoss, M. J. (2010). Effect of collision energy optimization on the measurement of peptides by selected reaction monitoring (SRM) mass spectrometry. *Analytical Chemistry*, *82*, 10116–10124.

Malatinszky, D., Steuer, R., & Jones, P. R. (2017). A comprehensively curated genome-scale two-cell model for the heterocystous cyanobacterium *Anabaena* sp. PCC 7120. *Plant Physiology*, *173*, 509–523.

Martín-Figueroa, E., Navarro, F., & Florencio, F. J. (2000). The GS-GOGAT pathway is not operative in the heterocysts. Cloning and expression of glsF gene from the cyanobacterium *Anabaena* sp. PCC 7120. *FEBS Letters*, *476*, 282–286.

Maxwell, K., & Johnson, G. N. (2000). Chlorophyll fluorescence—A practical guide. *Journal of Experimental Botany*, *51*, 659–668.

Meeks, J. C., Wolk, C. P., & Lockau, W. (1978). Pathways of assimilation of [13N]N2 and 13NH4+ by cyanobacteria with and without heterocysts. *Journal of Bacteriology*, *134*, 125–130.

Merida, A., Candau, P., & Florencio, F. J. (1991). Regulation of glutamine synthetase activity in the unicellular cyanobacterium *Synechocystis* sp. strain PCC 6803 by the nitrogen source: Effect of ammonium. *Journal of Bacteriology*, *173*, 4095–4100.

Merino-Puerto, V., Mariscal, V., Mullineaux, C. W., Herrero, A., & Flores, E. (2010). Fra proteins influencing filament integrity, diazotrophy and localization of septal protein SepJ in the heterocyst-forming cyanobacterium *Anabaena* sp. *Molecular Microbiology*, *75*, 1159–1170.

Messineo, L. (1966). Modification of the Sakaguchi reaction: Spectrophotometric determination of arginine in proteins without previous hydrolysis. *Archives of Biochemistry and Biophysics*, *117*, 534–540.

Michopoulos, F. (2018). Ion pair chromatography for endogenous metabolites LC-MS analysis in tissue samples following targeted acquisition. In G. Theodoridis H. Gika & I. Wilson (eds.). *Methods in molecular biology* (pp. 1738, 83–97). New York, NY: Humana Press Inc.

Mo, R., Yang, M., Chen, Z., Cheng, Z., Yi, X., Li, C., … Ge, F. (2015). Acetylome analysis reveals the involvement of lysine acetylation in photosynthesis and carbon metabolism in the model cyanobacterium *Synechocystis* sp. PCC 6803. *Journal of Proteome Research*, *14*, 1275–1286.

Montesinos, M. L., Herrero, A., & Flores, E. (1997). Amino acid transport in taxonomically diverse cyanobacteria and identification of two genes encoding elements of a neutral amino acid permease putatively involved in recapture of leaked hydrophobic amino acids. *Journal of Bacteriology*, *179*, 853–862.

Montesinos, M. L., Muro-Pastor, A. M., Herrero, A., & Flores, E. (1998). Ammonium/methylammonium permeases of a cyanobacterium: Identification and analysis of three nitrogen-regulated amt genes in *Synechocystis* sp. PCC 6803. *Journal of Biological Chemistry*, *273*, 31463–31470.

Mullineaux, C. W., Mariscal, V., Nenninger, A., Khanum, H., Herrero, A., Flores, E., & Adams, D. G. (2008). Mechanism of intercellular molecular exchange in heterocyst-forming cyanobacteria. *EMBO Journal*, *27*, 1299–1308.

Muro-Pastor, A. M., & Hess, W. R. (2012). Heterocyst differentiation: From single mutants to global approaches. *Trends in Microbiology*, *20*, 548–557.

Muro-Pastor, M. I., Reyes, J. C., & Florencio, F. J. (2001). Cyanobacteria perceive nitrogen status by sensing intracellular 2-oxoglutarate levels. *The Journal of Biological Chemistry*, *276*(41), 38320–38328.

Murton, J., Nagarajan, A., Nguyen, A. Y., Liberton, M., Hancock, H. A., Pakrasi, H. B., & Timlin, J. A. (2017). Population-level coordination of pigment response in individual cyanobacterial cells under altered nitrogen levels. *Photosynthesis Research*, *134*, 165–174.

Nakayasu, E. S., Burnet, M. C., Walukiewicz, H. E., Wilkins, C. S., Shukla, A. K., Brooks, S., … Payne, S. H. (2017). Ancient regulatory role of lysine acetylation in central metabolism. *mBio*, *8*(6), e01894–17.

Narainsamy, K., Farci, S., Braun, E., Junot, C., Cassier-Chauvat, C., & Chauvat, F. (2016). Oxidative-stress detoxification and signalling in cyanobacteria: The crucial glutathione synthesis pathway supports the production of ergothioneine and ophthalmate. *Molecular Microbiology*, *100*, 15–24.

Nicolaisen, K., Hahn, A., & Schleiff, E. (2009). The cell wall in heterocyst formation by *Anabaena* sp. PCC 7120. *Journal of Basic Microbiology*, *49*, 5–24.

Nürnberg, D. J., Mariscal, V., Bornikoel, J., Nieves-Morión, M., Krauß, N., Herrero, A., … Mullineaux, C. W. (2015). Intercellular diffusion of a fluorescent sucrose analog via the septal junctions in a filamentous cyanobacterium. *mBio*, *6*, e02109.

Omata, T., Andriesse, X., & Hirano, A. (1993). Identification and characterization of a gene cluster involved in nitrate transport in the cyanobacterium *Synechococcus* sp. PCC7942. *Molecular and General Genetics MGG*, *236*, 193–202.

Orr, J., Keefer, L. M., Keim, P., Nguyen, T. D., Wellems T., Heinrikson, R. L., & Haselkorn, R. (1981). Purification, physical characterization, and NH_2-terminal sequence of glutamine synthetase from the cyanobacterium *Anabaena* 7120. *The Journal of Biological Chemistry*, *256*(24), 13091–13098.

Paz-Yepes, J., Herrero, A., & Flores, E. (2007). The NtcA-regulated amtB gene is necessary for full methylammonium uptake activity in the cyanobacterium *Synechococcus elongatus*. *Journal of Bacteriology*, *189*, 7791–7798.

Paz-Yepes, J., Merino-Puerto, V., Herrero, A., & Flores, E. (2008). The amt gene cluster of the heterocyst-forming cyanobacterium *Anabaena* sp. strain PCC 7120. *Journal of Bacteriology*, *190*, 6535–6539.

Percival, S. L., & Williams, D. W. (2013). Cyanobacteria. In *Microbiology of waterborne diseases: Microbiological aspects and risks* (2nd ed., pp. 79–88). London: Elsevier Ltd.

Perin, G., Bellan, A., Segalla, A., Meneghesso, A., Alboresi, A., & Morosinotto, T. (2015). Generation of random mutants to improve light-use efficiency of *Nannochloropsis gaditana* cultures for biofuel production. *Biotechnology for Biofuels*, *8*, 161.

Perin, G., Yunus, I. S., Valton, M., Alobwede, E., & Jones, P. R. (2019). Sunlight-driven recycling to increase nutrient use-efficiency in agriculture. *Algal Research*, *41*, 101554.

Picossi, S., Flores, E., & Herrero, A. (2014). ChIP analysis unravels an exceptionally wide distribution of DNA binding sites for the NtcA transcription factor in a heterocyst-forming cyanobacterium. *BMC Genomics*, *15*, 22.

Picossi, S., Montesinos, M. L., Pernil, R., Lichtlé, C., Herrero, A., & Flores, E. (2005). ABC-type neutral amino acid permease N-I is required for optimal diazotrophic growth and is repressed in the heterocysts of *Anabaena* sp. strain PCC 7120. *Molecular Microbiology*, *57*, 1582–1592.

Rascio, N., & La Rocca, N. (2013). Biological nitrogen fixation. In B. Fath (ed.). *Reference module in earth systems and environmental sciences*. (Encyclopedia of Ecology (Second Edition), 2, 2, 264–279). Amsterdam, Netherlands: Elsevier.

Reitzer, L. (2003). Nitrogen assimilation and global regulation in *Escherichia coli*. *Annual Review of Microbiology*, *57*, 155–176.

Rippka, R., Deruelles, J., & Waterbury, J. B. (1979). Generic assignments, strain histories and properties of pure cultures of cyanobacteria. *Journal of General Microbiology*, *111*, 1–61.

Ritchie, R. J. (2006). Consistent sets of spectrophotometric chlorophyll equations for acetone, methanol and ethanol solvents. *Photosynthesis Research*, *89*, 27–41.

Robinson, C. (2017). Phytoplankton biogeochemical cycles. In C. Castellani & M. Edwards (Eds.), *Marine plankton: A practical guide to ecology, methodology, and taxonomy* (pp. 42–52). Oxford, UK: Oxford University Press.

Simon, R. D. (1973). Measurement of the cyanophycin granule polypeptide contained in the blue-green Alga *Anabaena cylindrica*. *Journal of Bacteriology*, *114*(3), 1213–1216.

Sinetova, M. A., Červený, J., Zavřel, T., & Nedbal, L. (2012). On the dynamics and constraints of batch culture growth of the cyanobacterium *Cyanothece* sp. ATCC 51142. *Journal of Biotechnology*, *162*, 148–155.

Singh, S. P., & Montgomery, B. L. (2011). Determining cell shape: Adaptive regulation of cyanobacterial cellular differentiation and morphology. *Trends in Microbiology*, *19*, 278–285.

Thiel, T., & Pratte, B. (2001). Effect on heterocyst differentiation of nitrogen fixation in vegetative cells of the Cyanobacterium *Anabaena variabilis* ATCC 29413. *Journal of Bacteriology*, *183*, 280–286.

Tremblay, P. L., & Hallenbeck, P. C. (2008). Ammonia-induced formation of an AmtB-GlnK complex is not sufficient for nitrogenase regulation in the photosynthetic bacterium *Rhodobacter capsulatus*. *Journal of Bacteriology*, *190*, 1588–1594.

Valladares, A., Maldener, I., Muro-Pastor, A. M., Flores, E., & Herrero, A. (2007). Heterocyst development and diazotrophic metabolism in terminal respiratory oxidase mutants of the cyanobacterium *Anabaena* sp. strain PCC 7120. *Journal of Bacteriology*, *189*, 4425–4430.

Valladares, A., Montesinos, M. L., Herrero, A., & Flores, E. (2002). An ABC-type, high-affinity urea permease identified in cyanobacteria. *Molecular Microbiology*, *43*, 703–715.

Valladares, A., Rodríguez, V., Camargo, S., Martínez-Noël, G. M. A., Herrero, A., & Luque, I. (2011). Specific role of the cyanobacterial pipX factor in the heterocysts of *Anabaena* sp. strain PCC 7120. *Journal of Bacteriology*, *193*, 1172–1182.

Wang, S., Orabi, E. A., Baday, S., Bernèche, S., & Lamoureux, G. (2012). Ammonium transporters achieve charge transfer by fragmenting their substrate. *Journal of the American Chemical Society*, *134*, 10419–10427.

Watzer, B., Engelbrecht, A., Hauf, W., Stahl, M., Maldener, I., & Forchhammer, K. (2015). Metabolic pathway engineering using the central signal processor PII. *Microbial Cell Factories*, *14*, 192.

Watzer, B., & Forchhammer, K. (2018). Cyanophycin synthesis optimizes nitrogen utilization in the unicellular cyanobacterium *Synechocystis* sp. strain PCC 6803. *Applied and Environmental Microbiology*, *84*(20), e01298–18.

Watzer, B., Spät, P., Neumann, N., Koch, M., Sobotka, R., Macek, B., … Forchhammer, K. (2019). The signal transduction protein PII controls ammonium, nitrate and urea uptake in cyanobacteria. *Frontiers in Microbiology*, *10*, 1428.

Wellburn, A. R. (1994). The spectral determination of chlorophylls a and b, as well as total carotenoids, using various solvents with spectrophotometers of different resolution. *Journal of Plant Physiology*, *144*, 307–313.

Willis, R. B., Montgomery, M. E., & Allen, P. R. (1996). Improved method for manual, colorimetric determination of total Kjeldahl nitrogen using salicylate. *Journal of Agricultural and Food Chemistry*, *44*, 1804–1807.

Yakunin, A. F., & Hallenbeck, P. C. (2002). AmtB is necessary for NH_4^+-induced nitrogenase switch-off and ADP-ribosylation in *Rhodobacter capsulatus*. *Journal of Bacteriology*, *184*, 4081–4088.

Zhang, C. C., Zhou, C. Z., Burnap, R. L., & Peng, L. (2018). Carbon/nitrogen metabolic balance: Lessons from cyanobacteria. *Trends in Plant Science*, *23*, 1116–1130.

SUPPORTING INFORMATION

Additional supporting information may be found online in the Supporting Information section at the end of this article.

How to cite this article: Perin G, Fletcher T, Sagi-Kiss V, et al. Calm on the surface, dynamic on the inside. Molecular homeostasis of *Anabaena* sp. PCC 7120 nitrogen metabolism. *Plant Cell Environ*. 2021;1–23. https://doi.org/10.1111/pce.14034